Journal of Visualized Experiments

Multitimescale Microscopy Methods for the Characterization of Fluorescently Labeled Microbubbles for Ultrasound-triggered Drug Release

--Manuscript Draft--

Article Type:	Invited Methods Collection - JoVE Produced Video
Manuscript Number:	JoVE62251R1
Full Title:	Multitimescale Microscopy Methods for the Characterization of Fluorescently Labeled Microbubbles for Ultrasound-triggered Drug Release
Corresponding Author:	Charlotte Nawijn University of Twente Enschede, NETHERLANDS
Corresponding Author's Institution:	University of Twente
Corresponding Author E-Mail:	c.l.nawijn@utwente.nl
Order of Authors:	Charlotte Louise Nawijn
	Tim Segers
	Guillaume Lajoinie
	Ýrr Mørch
	Sigrid Berg
	Sofie Snipstad
	Catharina de Lange Davies
	Michel Versluis
Additional Information:	
Question	**Response**
Please specify the section of the submitted manuscript.	Bioengineering
Please indicate whether this article will be Standard Access or Open Access.	Open Access (US$4,200)
Please indicate the **city, state/province, and country** where this article will be **filmed**. Please do not use abbreviations.	Enschede, Overijssel, the Netherlands, and Trondheim, Trøndelag, Norway
Please confirm that you have read and agree to the terms and conditions of the author license agreement that applies below:	I agree to the Author License Agreement
Please provide any comments to the journal here.	

TITLE:

Multitimescale Microscopy Methods for the Characterization of Fluorescently Labeled Microbubbles for Ultrasound-triggered Drug Release

AUTHORS AND AFFILIATIONS:

Charlotte Nawijn*[1], Tim Segers[1,2], Guillaume Lajoinie[1], Ýrr Mørch[3], Sigrid Berg[4,5,6], Sofie Snipstad[3,6,7], Catharina de Lange Davies[7], Michel Versluis[1]

[1]Physics of Fluids group, Department of Science and Technology, MESA+ Institute for Nanotechnology and Technical Medical (TechMed) Center, University of Twente, Enschede, the Netherlands
[2]BIOS Lab-on-a-Chip group, Max Planck Center Twente for Complex Fluid Dynamics, MESA+ Institute for Nanotechnology and Technical Medical (TechMed) Center, University of Twente, Enschede, the Netherlands
[3]Department of Biotechnology and Nanomedicine, SINTEF Industry, Trondheim, Norway
[4]Department of Circulation and Medical Imaging, Norwegian University of Science and Technology, Trondheim, Norway
[5]Department of Health Research, SINTEF Digital, Trondheim, Norway
[6]Cancer Clinic, St. Olav's Hospital, Trondheim, Norway
[7]Department of Physics, Norwegian University of Science and Technology, Trondheim, Norway

Emails of co-authors:

Tim Segers	t.j.segers@utwente.nl
Guillaume Lajoinie	g.p.r.lajoinie@utwente.nl
Ýrr Mørch	yrr.morch@sintef.no
Sigrid Berg	sigrid.berg@sintef.no
Sofie Snipstad	sofie.snipstad@ntnu.no
Catharina de Lange Davies	catharina.davies@ntnu.no
Michel Versluis	m.versluis@utwente.nl

Corresponding author:

Charlotte Nawijn c.l.nawijn@utwente.nl

KEYWORDS:

ultrasound, ultrasound contrast agents, drug delivery, bright-field microscopy, fluorescence microscopy, intravital microscopy, confocal microscopy

SUMMARY:

The presented protocols can be used to characterize the response of fluorescently labeled microbubbles designed for ultrasound-triggered drug delivery applications, including their activation mechanisms as well as their bioeffects. This paper covers a range of *in vitro* and *in vivo* microscopy techniques performed to capture the relevant length and timescales.

ABSTRACT:

Microbubble contrast agents hold great promise for drug delivery applications with ultrasound. Encapsulating drugs in nanoparticles reduces systemic toxicity and increases circulation time of the drugs. In a novel approach to microbubble-assisted drug delivery, nanoparticles are incorporated in or on microbubble shells, enabling local and triggered release of the nanoparticle payload with ultrasound. A thorough understanding of the release mechanisms within the vast ultrasound parameter space is crucial for efficient and controlled release. This set of presented protocols is applicable to microbubbles with a shell containing a fluorescent label. Here, the focus is on microbubbles loaded with poly(2-ethyl-butyl cyanoacrylate) polymeric nanoparticles, doped with a modified Nile Red dye. The particles are fixed within a denatured casein shell. The microbubbles are produced by vigorous stirring, forming a dispersion of perfluoropropane gas in the liquid phase containing casein and nanoparticles, after which the microbubble shell self-assembles. A variety of microscopy techniques are needed to characterize the nanoparticle-stabilized microbubbles at all relevant timescales of the nanoparticle release process. Fluorescence of the nanoparticles enables confocal imaging of single microbubbles, revealing the particle distribution within the shell. *In vitro* ultra-high-speed imaging using bright-field microscopy at 10 million frames per second provides insight into the bubble dynamics in response to ultrasound insonation. Finally, nanoparticle release from the bubble shell is best visualized by means of fluorescence microscopy performed at 500,000 frames per second. To characterize drug delivery *in vivo*, the triggered release of nanoparticles within the vasculature and their extravasation beyond the endothelial layer is studied using intravital microscopy in tumors implanted in dorsal skinfold window chambers, over a timescale of several minutes. The combination of these complementary characterization techniques provides unique insight into the behavior of microbubbles and their payload release at a range of time and length scales, both *in vitro* and *in vivo*.

INTRODUCTION:

Ultrasound is the most widely used medical imaging technique. It is non-invasive, fast, safe, cost-effective, and portable[1–3]. However, blood is a poor ultrasound scatterer, and the contrast of the blood pool can be enhanced by an intravenous injection of ultrasound contrast agents[3]. This enhanced blood-pool contrast enables the quantification of organ perfusion for diagnostic purposes, *e.g.*, in the detection of coronary artery disease[4] and metastatic liver disease[5]. Indeed, tumor vasculature was proven to be an important prognostic factor[6]. A major research effort is now directed towards microbubble-assisted, targeted molecular imaging and tailoring contrast agents for therapeutic use. Commercially available ultrasound contrast agents typically consist of a suspension of coated microbubbles[7,8] with diameters ranging from 1 µm to 10 µm[9]. As ultrasound contrast agent microbubbles are slightly smaller than red blood cells[7], the microbubbles can safely reach even the smallest capillaries without creating an occlusion[3]. Microbubbles have a dramatically increased ultrasound backscattering coefficient compared to tissue[10], owing to their compressible gas core[11]. Furthermore, the microbubble echo is highly nonlinear, *i.e.*, its spectrum contains harmonics and subharmonics of the driving frequency. In addition, the echo strength is strongly dependent on the resonant response of the bubble[12].

While tissue scatters only linearly, a small number of microbubbles is sufficient to achieve a high detection sensitivity in harmonic imaging[13,14]. This nonlinear contrast generation can even be

strong enough to track single bubbles in the body[15]. The shell of the ultrasound contrast agent stabilizes the bubbles against dissolution and coalescence, thereby increasing their circulation time in the blood pool[16]. The shell can consist of lipids, polymers, or denatured proteins[3,8]. It decreases the interfacial tension, thereby limiting the effect of Laplace pressure-driven dissolution[17] and creates a resistive barrier against gas diffusion[18]. To further increase stability, the contrast microbubbles are typically filled with a high-molecular weight gas with low solubility in blood[11]. The microbubble shell dramatically changes the response of the microbubbles to ultrasound insonation[11]. Although free gas bubbles have a characteristic resonance frequency that is inversely proportional to their size, the addition of a lipid coating increases the resonance frequency of the bubbles owing to the intrinsic stiffness of the shell[3]. Furthermore, the shell dissipates energy through dilatational viscosity, which constitutes the dominant source of damping for coated bubbles[3]. The stabilizing shell has the additional advantage that it can be functionalized, *e.g.,* by binding targeting ligands to the surface of microbubbles. This targeting enables many applications for these bubbles and, in particular, molecular imaging with ultrasound[14,19]. Microbubble contrast agents hold great promise for drug delivery applications with ultrasound.

Microbubbles oscillating in the confinement of a blood vessel can cause microstreaming as well as local normal and shear stresses on the capillary wall[3]. At high acoustic pressures, large amplitude oscillations may lead to microbubble collapse in a violent process termed inertial cavitation, which, in turn, may lead to rupture or invagination of the blood vessel[20]. These violent phenomena can induce bioeffects such as sonopermeation[21], enhancing the extravasation of therapeutic drugs into the interstitium across the endothelial wall, either paracellularly or transcellularly. It may also improve the penetration of therapeutic agents through the extracellular matrix of stroma-rich tumors[21,22] and biofilms[23,24], although this mechanism is still poorly understood[26]. Ultrasound-mediated drug delivery has shown promising results both preclinically[27,28] and in clinical trials[22]. Moreover, when used with relatively low-frequency ultrasound (~1 MHz), microbubbles have been reported to locally and transiently increase the blood-brain barrier permeability, thereby enabling drugs to enter the brain parenchyma, both in preclinical and clinical studies[29–34]. There are generally two approaches to ultrasound-mediated drug delivery: the therapeutic material can be co-administered with the bubbles, or it can be attached to or loaded in the bubble shell[28,35,36]. The second approach has been shown to be more efficient in terms of drug delivery[37]. Microbubbles can be loaded with drugs or genetic material encapsulated in nanoparticles (liposomes or polymeric nanoconstructs) attached to the shell or incorporated directly in the microbubble shell[35,36]. Nanoparticle-loaded microbubbles can be activated by (focused) ultrasound to locally release the nanoparticle payload[28,33,38–40].

If such a microbubble is in direct contact with a cell, it has been shown *in vitro* that the payload can even be deposited onto the cell cytoplasmic membrane in a process called sonoprinting[34,35]. The ultrasound parameter space for microbubble insonation is extensive, and the *in vivo* biological conditions further add complexity. Thus, the combination of focused ultrasound and nanoparticle-loaded microbubbles poses a challenge in the field of targeted therapeutics. The aim of this work is to provide protocols that can be used to image, in detail, the response of microbubbles as a function of the ultrasound parameters and to study the mechanisms leading

to shell rupture and subsequent release of the fluorescently labeled shell material. This set of protocols is applicable to microbubbles with shells that contain a fluorescent dye. **Figure 1** shows a schematic representation of the polymeric-nanoparticle-and-protein-stabilized microbubbles developed at SINTEF (Trondheim, Norway). These bubbles are filled with perfluoropropane gas (C_3F_8) and the nanoparticles that stabilize the shell contain NR668, which is a lipophilic derivative of Nile Red fluorescent dye[38,43]. The nanoparticles consist of poly(2-ethyl-butyl cyanoacrylate) (PEBCA) and are PEGylated. Functionalization with polyethylene glycol (PEG) reduces opsonization and phagocytosis by the mononuclear phagocyte system, thereby extending the circulation time[14,44]. As a result, PEGylation increases the amount of nanoparticles reaching the target site, thereby improving the efficacy of the treatment[16].

Figure 2 illustrates how the use of four microscopy methods allows researchers to cover all relevant time and length scales. It should be noted that the spatial resolution achievable in optical microscopy is determined by the diffraction limit, which depends on the wavelength of the light and numerical aperture (NA) of the objective (or of the object illumination source)[45]. For the systems at hand, the optical resolution limit is typically 200 nm. Additionally, intravital microscopy can be used to image on the subcellular level[46]. For the nanoparticle-and-protein-stabilized microbubbles used in this work, the minimum length scale relevant for intravital microscopy is the size of small capillaries (≥10 μm). *In vitro* high-speed optical imaging (10 million frames per second) and high-speed fluorescence imaging (500,000 frames per second) experiments are described for single microbubbles. High-speed bright-field imaging at nanosecond timescales is suitable to study the time-resolved radial dynamics of the vibrating bubbles. In contrast, high-speed fluorescence microscopy allows for direct visualization of the release of the fluorescently labeled nanoparticles. Furthermore, the structure of the microbubble shell can be investigated using Z-stack three-dimensional (3D) confocal microscopy, and scanning electron microscopy (the protocol for the latter is not included in the current work). Intravital microscopy consists in using multi-photon microscopy to image tumors growing in dorsal window chambers to provide real-time information on local blood flow and on the fate of fluorescently-labeled nanoparticles *in vivo*[47]. The combination of these microscopy methods ultimately provides detailed insight into the behavior of therapeutic microbubble agents in response to ultrasound, both *in vitro* and *in vivo*.

PROTOCOL:

NOTE: All experimental procedures were approved by the Norwegian Animal Research Authorities. Details of materials that were used in the protocol can be found in the **Table of Materials**.

1. Production of microbubbles

NOTE: In this work, the microbubbles of interest are protein-and-nanoparticle-stabilized microbubbles, for which the production protocol has been described previously[28,33,48]. Therefore, the fabrication protocol has been briefly summarized here. First, using a pipette, mix ultrapure water with 0.5 wt% of casein in phosphate-buffered saline (PBS) and 1 wt% of the nanoparticles

labeled with 0.21 wt% of the fluorescent dye, NR668 (modified Nile Red), in a sterile glass crimp top vial (10 mL, diameter of 2 cm). The polymeric nanoparticles are prepared using the mini-emulsion polymerization method as described by Mørch *et al*.[38]. Here, the dye functions as a model drug to enable visualization of nanoparticle release. When working with the nanoparticle solution, wear a lab coat, goggles, and gloves. Wipe away any spills of the nanoparticle solution immediately with 100% acetone.

1.1. Cap the vial with the rubber cap, mix slightly, and place the vial in an ultrasonic bath for 10 min at room temperature to eliminate possible aggregates. Place a dispersion tool with the tip of the stirrer ~0.5 cm from the bottom of the glass vial. Using a glass pipette connected to the gas container, add the perfluoropropane gas to the head space of the vial containing the solution until the solution starts bubbling slightly.

NOTE: Wrap self-sealing film around the base of the dispersion tool to prevent slipping of the glass vial during stirring.

1.2. Stir the solution vigorously at 1935 × *g* (24,000 rpm with a radius of rotation of 3 mm) for 4 min using the dispersion tool. Close the vial with the rubber cap, and seal the vial for further use.

NOTE: The stirring entraps the gas in the liquid. The microbubble-shell subsequently self-assembles without requiring any additional step.

1.3. Store the excess casein and nanoparticle solution at 4 °C, and clean the dispersion tool with 100% acetone.

2. Imaging single bubbles

2.1. Confocal microscopy

2.1.1. Sample preparation

2.1.1.1. Dilute the bubble solution to image single microbubbles. Place a venting needle (19 G–21 G) in a glass crimp top vial containing the microbubbles produced by following the procedure described in section 1. Turn the vial upside down to allow large bubbles to move away from the seal of the vial.

2.1.1.2. Insert another needle tip (19 G) of a small (~1 mL) syringe into the vial, while the vial is still upside down. Remove a small amount of the bubble suspension, and transfer the contents of the syringe into a small tube for easier pipetting in the next step.

NOTE: The volume of the suspension to extract directly depends on the type and concentration of the bubble suspension. In this case, 0.2 mL was extracted.

2.1.1.3. Using a pipette, dilute the microbubble suspension (from section 1) in filtered PBS to

achieve a concentration of approximately 2 × 10^5 to 6 × 10^5 microbubbles/mL and to enable single-bubble imaging.

NOTE: Depending on the bubble type, it is recommended to wash the bubble suspension to remove free fluorescent dye. This is particularly important with bubbles for which the fluorescent dye is infused in the shell. To wash bubbles, dilute the bubble suspension (*e.g.,* by taking 100 µL of the bubble solution in 10 mL of PBS), and centrifuge it (typically at speeds of the order of 100 × *g*). Finally, remove the supernatant containing the microbubbles with a pipette for further analysis. The remaining solution contains the free fluorescent particles and can be discarded. The washing step should be repeated as necessary.

2.1.1.4. Add glycerol to the mixture to increase the viscosity of the medium and eliminate the movement induced by Brownian motion that would otherwise interfere with the rather slow confocal Z-stack imaging.

NOTE: The amount of glycerol depends on the type of bubble that is imaged (here, ~50%). For some types of bubbles, glycerol might have an adverse effect on stability[49]. However, no noticeable change was observed in the bubbles over approximately 30 min under confocal imaging. Furthermore, glycerol affects the acoustic response of microbubbles and can therefore only be used with imaging methods where the microbubbles are not insonified.

2.1.1.5. Place the microbubble suspension in a chamber with thin walls for optimal imaging such as a channel slide.

2.1.2. Imaging protocol

2.1.2.1. Switch on the confocal microscope, and select a suitable objective and the desired laser and scanner to use during confocal microscopy.

NOTE: Here, a use a 60x water immersion objective for a resolution of 0.08 µm/pixel and depending on the bubble size, image a region of 256 x 256 pixels or 128 x 128 pixels. In these specific experiments, use a 488 nm laser line and a Galvano scanner. The emission wavelength depends on the fluorescent dye and is typically broadband.

2.1.2.2. Find a microbubble in bright-field, and switch to confocal microscopy. Set the desired top and bottom planes in between which the confocal microscope will scan. Acquire a Z-stack to observe the 3D structure; use a step size of 100 nm in the Z-direction.

2.2. Bright-field microscopy

2.2.1. Assembly of the optical system

NOTE: A schematic representation of the bright-field microscopy setup is shown in **Figure 3A**. To ensure proper ultrasound propagation, the water bath contains two openings: one for a light

source and one for an ultrasound transducer. The optical system consists of a (modular) microscope, a high-speed camera, and appropriate optics. As the period of microbubble oscillations is typically of the order of 1 µs (using 1 MHz ultrasound), the camera should be set to record at a framerate of at least 5 million frames per second. Here, the camera is to be set to record at 10 million frames per second (256 x 400 pixels) for 256 frames (25.6 µs) to capture all details of the bubble dynamics including higher harmonics.

2.2.1.1. Attach a water immersion objective with an appropriate magnification, working distance, and NA to the microscope.

NOTE: A water immersion objective was used to provide a stable working distance despite gradual evaporation of the water. Here, a water immersion objective with a magnification of 60x, a working distance of 2 mm, and an NA of 1 was selected.

2.2.1.2. Use a strobe light with a peak power output of at least 1 kW for illumination and a tube lens between the microscope and the camera to ensure that as little ambient light as possible reaches the sensor of the high-speed camera.

2.2.1.3. Use a dimmable halogen light source for focusing on single microbubbles and alignment of the optical and acoustical system for real-time imaging.

2.2.2. Assembly of the acoustical system

2.2.2.1. Use a programmable arbitrary waveform generator and a power-amplifier (56 dB gain) to drive the transducer with a smooth envelop and waveform. Connect an oscilloscope to the arbitrary waveform generator to check the signal. Connect a personal computer to the arbitrary waveform generator to program the incoming acoustic pressure wave, using a script written in-house.

2.2.2.2. Use a pulse/delay generator as master trigger to synchronize the optical and acoustical systems. Set the trigger delays on the pulse/delay generator and the camera software so that the recording starts 16 µs after ultrasound generation to allow the ultrasound wave to reach the bubbles. Trigger the light source 1.5 µs before the start of the recording to ensure proper illumination during the bubble oscillations (see **Figure 3B** for the timing diagram).

2.2.2.3. Choose a suitable transducer with an appropriate center frequency. Place it in an opening of the water bath, so that it is at an angle with respect to the optical axis to minimize reflections from the sample holder membranes and to reduce standing wave formations. Calibrate the transfer function from voltage amplitude to pressure amplitude of the transducer using a fiber optic hydrophone as a function of the ultrasound frequency.

NOTE: Here, a single-element focused immersion transducer with a center frequency of 2.25 MHz, a focal distance of 1" and element diameter of 0.75" was placed at an angle of 35° with respect to the optical axis. The calibration of the transfer function needs to be performed using

the amplifier used in the acoustical system.

2.2.3. Choosing the sample holder

2.2.3.1. Use a sample holder with optically and acoustically transparent membranes and a volume that is large enough to allow for imaging of several single microbubbles within the same sample.

NOTE: Here, a cell culture cassette with a volume of 10 mL, membrane areas of 25 cm^2, and membrane thickness of 175 µm was used. Due to acoustic reflections on the lower membrane, and interference from waves reflected by the microscope objective and the upper membrane, the *in situ* acoustic pressure might differ from that programmed on the arbitrary waveform generator. Placing the transducer at an angle with respect to the sample holder membranes reduces standing wave formation, but can increase reflections from the membranes.

2.2.3.2. Ensure the sample can be fully submerged and brought within the focus of both the transducer and the microscope objective. Use an aluminum support attached to a 3D micropositioning stage to move the sample holder independently.

2.2.4. Alignment of the optical and acoustical systems

2.2.4.1. For 3D translation to align the setup, attach the water bath to an XY-translation stage, and attach the stage to an optical table to ensure it does not move during experiments. Then, fill the water bath with water, and switch on the dimmable halogen light source. During alignment, move the microscope objective to the side to prevent ultrasound reflections.

2.2.4.2. Attach a needle hydrophone (0.2 mm) to the sample holder arm, and place the needle hydrophone in the water bath, with the tip in the field of view of the objective. Turn on the amplifier and the arbitrary waveform generator; use single pulses of 5 to 10 ultrasound cycles and a pulse repetition frequency of 15 Hz. Make sure that the hydrophone tip is focused and centered on the microscope image. Move the tank in the XY-direction and the needle in the Z-direction until the maximum pressure amplitude is reached.

2.2.4.3. Adjust the focus of the microscope to refocus on the tip of the hydrophone.

NOTE: This protocol ensures the alignment between the microscope focus and the transducer focus. Do not change the position of the microscope and the transducer after alignment.

2.2.5. Sample preparation

2.2.5.1. Repeat steps 2.1.1.1 through 2.1.1.3 to prepare the sample solution. Dilute the bubble solution to enable single-bubble imaging and to rule out acoustic interactions of neighboring bubbles.

2.2.5.2. Open the outlet of the sample holder. Using a syringe, inject the sample solution into the other opening of the sample holder until it is completely filled. Ensure that there are no air bubbles inside the sample holder to prevent unwanted interactions with the ultrasound field.

2.2.5.3. Close both valves of the sample holder, and place the sample holder perpendicular to the optical axis.

NOTE: Keep the filled sample holder level to prevent shifting of the bubbles to one side of the sample holder during moving.

2.2.6. Imaging protocol

2.2.6.1. Program the desired ultrasound driving frequency and acoustic pressure in the arbitrary waveform generator through the aforementioned in-house written script.

NOTE: Here, the acoustic pressure wave was a single burst of 40 cycles, with an 8-cycle Gaussian-tapered pulse. Ultrasound frequencies used in these experiments were 1 MHz, 2 MHz, or 3 MHz, with acoustic pressure amplitudes ranging from 81 kPa to 1200 kPa.

2.2.6.2. Move the sample holder containing the sample solution using the XYZ-stage to locate single microbubbles in the focus of the microscope. Start with a field of view at a corner of the sample holder, and ensure that the edge of the microbubbles is clearly visible and in focus (see **Figure 3C** for an ideal camera view).

2.2.6.3. Attach the end of an optical fiber that was previously connected to the halogen light to a strobe light, so that the other end is still connected to the water bath. Trigger the recording.

2.2.6.4. Repeat steps 2.2.6.2 through 2.2.6.3 as many times as desired per ultrasound setting (frequency and acoustic pressure), moving the cell culture cassette containing the microbubbles at least 2 mm (in the focal plane) from the previous location to ensure the microbubbles in the field of view are not sonicated in previous experiments.

NOTE: Here, each experiment was repeated ~20 times. When the whole sample holder is insonified, empty the sample holder, and refill it with fresh sample solution for subsequent experiments.

2.2.7. Data analysis

2.2.7.1. Adopt a programming environment to perform data analysis according to the research question, and perform edge detection after processing the images. Using a function that measures properties of image regions, find the centroid of a bubble and the derivative of the intensity profile around each bubble to detect the edge of the bubble (and thus, the bubble radius R). Extract relevant parameters from the radius over time for single microbubbles.

NOTE: In the present study, a programming environment was used for image processing to binarize and filter recordings of single microbubbles. An in-house script was used to find the derivative of the intensity profile around each bubble.

2.3. Fluorescence microscopy

2.3.1. Assembly of the optical system

2.3.1.1. Build the setup for fluorescence microscopy (**Figure 4A**), with the same base used in the bright-field microscopy described in section 2.2.

NOTE: The setup described in section 2.3 can be combined with that described for bright-field microscopy in section 2.2. Combining both fluorescence microscopy and bright-field microscopy enables visualization of the microbubble gas core while imaging the nanoparticle release.

2.3.1.2. Set the high-speed camera to record at 500,000 frames per second (400 x 250 pixels) for 128 frames (256 µs).

NOTE: The imaging time is longer than in the bright-field experiments as the light intensity is limited in fluorescence, and because the timescale over which particle delivery occurs is longer than that of the bubble dynamics.

2.3.1.3. Select a laser with power high enough to supply sufficient light and that has a suitable excitation wavelength, and ensure that it is coupled with an acousto-optic modulator to avoid bleaching the sample.

NOTE: In this study, a 5 W continuous wave laser with an excitation wavelength of 532 nm was used to excite the fluorescence of the nanoparticles.

2.3.1.4. Place a beam splitter and band-stop filter between the laser and the microscope objective to direct the excitation light towards the sample while allowing the fluorescence emission to reach the camera.

2.3.2. Assembly of the acoustical system

2.3.2.1. To insonify the microbubbles, use the same acoustical setup as in section 2.2.2. Change the transducer in these specific experiments to a single-element, focused immersion transducer with a center frequency of 2.25 MHz, a focal distance of 1.88", and element diameter of 1". Place it at an angle of 35° with respect to the optical axis to minimize reflections from the sample holder membranes and reduce standing wave formations.

2.3.3. Alignment of the optical and acoustical systems

2.3.3.1. Repeat steps described in section 2.2.4.

2.3.4. Sample preparation

2.3.4.1. Prepare the sample solution as described in section 2.2.5.

2.3.5. Imaging protocol

2.3.5.1. Set the desired ultrasound driving frequency and acoustic pressure amplitude on the arbitrary waveform generator through the aforementioned in-house written script.

NOTE: Here, the acoustic pressure wave was programmed to be a single burst of ultrasound of 140 cycles, with a 10-cycle Gaussian-tapered pulse. Longer pulses are generally required to investigate drug delivery compared to bubble dynamics. Ultrasound frequencies used in these experiments were 1 MHz, 2 MHz, or 3 MHz, with acoustic pressure amplitudes ranging from 81 kPa to 1200 kPa.

2.3.5.2. On the pulse/delay generator, set the trigger delay for the laser for fluorescent excitation of the nanoparticles from the microbubbles during the recording.

NOTE: For these specific experiments, this trigger delay was between frames 10 (20 µs) and 85 (170 µs) for a total of 150 µs. The timing diagram is shown in **Figure 4B**.

2.3.5.3. Move the sample holder containing the sample solution using the XYZ-stage to locate single microbubbles in the focus of the microscope. Start with a field of view of a corner of the sample holder; see **Figure 4c** for an ideal camera view in which the edge of the microbubbles is clearly visible and in focus. Trigger the recording.

2.3.5.4. Repeat step 2.3.5.3 as many times as desired per ultrasound setting (frequency and acoustic pressure), moving the cell culture cassette containing the microbubbles at least 2 mm (in the focal plane) from the previous location to ensure microbubbles in the field of view are not sonicated in previous experiments.

NOTE: In this study, each experiment was repeated ~10–20x. When the whole sample holder is insonified, empty the sample holder, and refill it with fresh sample solution for subsequent experiments.

2.3.6. Data analysis

2.3.6.1. Analyze the fluorescence microscopy recordings according to the research question. For every microbubble, visually determine whether delivery of the nanoparticles in the FM experiments occurred. If detachment and deposition of the nanoparticles from the gas core onto the sample holder membrane is observed for a single microbubble, manually enter **delivery = true** in the programming environment.

3. Intravital microscopy

3.1. Dorsal skinfold window chamber surgery (described previously[26,47,50])

3.1.1. Acclimate the animals for one week before placing the window chambers. Although both female and male mice can be used, and age is unimportant, ensure that the weight of the mice is at least 22–24 g so that the skin is sufficiently flexible.

3.1.2. Perform the surgery under general anesthesia with intraoperative and postoperative analgesic treatment. Anesthetize the animal by a subcutaneous injection of fentanyl (0.05 mg/kg)/medetomidine (0.5 mg/kg)/midazolam (5 mg/kg)/water (2:1:2:5) at a dose of 0.1 mL per 10 g weight. Use a heating pad or a heating lamp to maintain the body temperature of the animal.

3.1.3. Pull gently on the double layer of skin on the back of the animal so that the skin is sandwiched between two symmetric polyoxymethylene frames of the window chamber. Fix the chamber by placing two screws extending through the double skin layer and suturing along the upper edge of the chamber.

3.1.4. Remove the skin within the circular frame of the chamber on one side of the skin fold. Place a cover glass with a diameter of 11.8 mm within the frame where the skin is removed to form a window into the tissue.

3.1.5. Use a subcutaneous injection of atipemazole (2.5 mg/kg), flumazenil (0.5 mg/kg), and water (1:1:8) at a dose of 0.1 mL per 10 g as antidote to terminate the anesthesia. Place the animal in a heated recovery rack overnight. Supplement the water for the animals with 25 mg/mL of enrofloxacin to prevent infection in the surgical site.

3.2. Tumor model creation

3.2.1. Maintain cancer cells at 37 °C and in a 5% CO_2 atmosphere in appropriate culture medium supplemented with 10% fetal bovine serum and 100 U/mL penicillin and 100 mg/mL streptomycin.

NOTE: The human osteosarcoma (OHS) cell line was used in this protocol, but other cell lines can also be used.

3.2.2. On the day after step 3.1.5, anesthetize the animal by isoflurane (5% during induction and 1–2% during maintenance) for a couple of minutes. Remove the cover glass, apply 5×10^6 cancer cells in 30 µL of cell culture medium, and replace the cover glass.

3.2.3. Allow the tumors to grow for 2 weeks before imaging, and monitor the weight and health status of the animals at least 3 times per week during this period.

3.3. Assembly of the optical system

3.3.1. Perform intravital imaging during ultrasound treatment (as described in previous work[26]) with a suitable microscope and objective depending on the research question in focus. See **Figure 5A** for a schematic representation of the experimental setup.

NOTE: For this specific experiment, a multiphoton microscope was used, equipped with a 20x water dipping objective (NA of 1.0 and working distance of 2 mm) and a pulsed laser. Images were acquired in resonant scanning mode at 31 frames per second (512 x 512 pixels) with a field of view of 400 x 400 µm. The excitation wavelength was 790 nm. The filters in front of the two gallium arsenide phosphide detectors were long pass 590 nm and bandpass 525/50 nm for the detection of fluorescence.

3.4. Assembly of the acoustical system

3.4.1. Mount a suitable ultrasound transducer in a wave guide (custom made) positioned below the objective at an angle of 45° with respect to the optical axis to minimize reflections from the cover glass of the dorsal skinfold window chamber and to reduce standing wave formations. Fill the wave guide with distilled and degassed water. Apply ultrasonic coupling gel on top of the wave guide.

3.5. Alignment of the optical and acoustical systems

3.5.1. Align the optical axis with the focus of the ultrasound. Position a fiber-optic hydrophone in the focus of the objective. Then, turn on the amplifier and the arbitrary waveform generator to excite the transducer with short bursts (5–10 cycles) with a pulse repetition frequency of 100 Hz, and move the ultrasound transducer to the position where the highest pressure is detected with the hydrophone on the oscilloscope.

NOTE: Do not change the position of the transducer after alignment.

3.6. Imaging protocol

3.6.1. Position the heated animal holder (custom design) connected to an XY-positioning stage between the wave guide and the objective, and add more coupling gel. Anesthetize the animal, and place a tail vein catheter. Place the mouse in the heated holder, and fix the window chamber in the holder. Add a water droplet on top of the cover slip in the window chamber, and move the objective in place to image the tumor tissue.

3.6.2. **Figure 5B** shows the timing diagram of the experiments depicting the order of events. Inject fluorescently labelled 2 MDa dextran intravenously (30 µL, 4 mg/mL diluted in saline) to visualize the vasculature, and move the mouse using the XY-translation stage to find a position with suitable blood vessels. Record baseline images before the ultrasound treatment. Adjust

frame rate, field of view, and length of recording depending on the research question and the specifics of the microscope and dyes to be imaged.

NOTE: In these experiments, 31 frames per second were recorded with a field of view of 400 x 400 µm, and imaging was done continuously for 5 min.

3.6.3. Set the desired ultrasound driving frequency, pulse length, and acoustic pressure amplitude on the arbitrary waveform generator.

NOTE: For these experiments, a frequency of 1 MHz was used with a pulse length of 10 ms and peak negative pressure amplitudes between 0.2 mPa and 0.8 mPa. A pulse repetition frequency of 0.5 Hz or 0.1 Hz was used to allow new microbubbles to reperfuse into the treated area between ultrasound pulses.

3.6.4. Inject 50 µL microbubbles (2×10^8 to 5×10^8 microbubbles/mL) intravenously, and apply ultrasound while imaging, as described in[26].

3.7. Data analysis

3.7.1. Depending on the research question, analyze images with (open source) image processing program and a programming environment, as described in[26], to determine blood vessel parameters (diameter, branching, flow speed, and direction), accumulation of nanoparticles in the vessels, and kinetics and penetration depth of extravasation of dextran and nanoparticles into tumor tissue.

REPRESENTATIVE RESULTS:

The microbubbles, produced as described in the protocol, were analyzed using various microscopy methods and at various timescales. The fluorescence of the nanoparticles in confocal microscopy (**Figure 6A**) indicates that the shell has a non-uniform particle distribution. Other microscopy methods can be used for bubble characterization. For example, **Figure 6B** shows the overall structure of the microbubble using scanning electron microscopy, as presented in previous work[34]. Radial dynamics and phenomenological bubble behavior can be studied using the described *in vitro* bright-field microscopy method wherein microbubbles were imaged at 10 million frames per second. The radius of single microbubbles was extracted over time using a script written in-house. An example of such a radial response is shown in **Figure 7**.

An image sequence of typical successful nanoparticle delivery, as described in section 2.3.6, is shown in **Figure 8a**. The nanoparticles embedded in the microbubble shell can be seen to light up due to fluorescence when the laser light reaches the bubble. Driven by ultrasound insonation, the fluorescent nanoparticles detach from the gas core of the microbubbles and are deposited on the membrane of the sample holder. Finally, the laser is turned off, and the fluorescent nanoparticles are no longer excited. Unsuccessful delivery of the fluorescently labeled payload of the microbubbles typically looks like the image sequence shown in **Figure 8b**, where the fluorescent nanoparticles light up on the shell of the microbubble that stays intact during

ultrasound exposure. Real-time intravital multiphoton microscopy during ultrasound was used to investigate the effects of ultrasound and microbubbles on nanoparticle behavior in the blood, enhancement of the permeability of tumor blood vessels, and improvement of the delivery of nanoparticles.

The extent and kinetics of penetration into the extracellular matrix as a function of acoustic pressure, frequency, and pulse lengths can be characterized. The effect of the ultrasound treatment may vary with respect to the size and morphology of the vessels and resulting confinement of the bubble. How the ultrasound treatment affects the blood flow and direction may be determined. An example experiment showing the extravasation of nanoparticles over time is shown in **Figure 9** at an mechanical index (MI) of 0.8[26]. Results of intravital multiphoton microscopy elucidate the spatial and temporal extravasation of nanoparticles during ultrasound exposure, which is highly beneficial for the complete understanding of the mechanisms underlying ultrasound-mediated delivery of nanoparticles and to optimize such technologies[26].

FIGURE LEGENDS:

Figure 1: Schematic representation of a microbubble with a shell of fluorescently labeled polymeric nanoparticles in denatured casein. The microbubbles are typically between 1 µm and 10 µm in diameter. The nanoparticles have a diameter mostly between 100 nm and 200 nm[38]. Abbreviation: C_3F_8 = perfluoropropane gas.

Figure 2: Schematic overview showing the relevant time and length scales for bright-field, fluorescence, confocal, and intravital microscopy.

Figure 3: Schematic representation of bright-field microscopy experiments. (**A**) Experimental setup, (**B**) the timing diagram, and (**C**) a typical recorded frame. Scale bar in (C) = 10 µm. Abbreviation: fps = frames per second.

Figure 4: Schematic representation of fluorescence microscopy experiments. (**A**) Experimental setup, (**B**) the timing diagram, and (**C**) a typical recorded frame. Scale bar in (C) = 10 µm. Abbreviation: fps = frames per second.

Figure 5: Schematic representation of intravital microscopy experiments. (**A**) Experimental setup, (**B**) the timing diagram, and (**C**) a typical recorded frame. Scale bar in (C) = 50 µm. Green corresponds to dextran-FITC and red to nanoparticles. Abbreviation: GaAsP = gallium arsenide phosphide.

Figure 6: 3D structure in scanning electron microscopic images of a nanoparticle-and-protein-stabilized microbubble. (**A**) Using confocal microscopy to show the nanoparticles, and (**B**) using a scanning electron microscope to show the 3D structure. (**B**) has been reproduced with permission from[34]. Scale bar in (**A**) = 5 µm; scale bar in (**B**) = 2 µm.

Figure 7: Typical spherical oscillations of a 2.89 µm radius nanoparticle-and-protein-stabilized microbubble insonified at an ultrasound frequency of 1 MHz and an acoustic pressure

amplitude of 142 kPa. (**A–D**) Images from the high-speed recording and the corresponding bubble radius over time curve (bottom). Scale bars = 5 µm, and the red line indicates the initial radius. The illumination profile (arbitrary units) is indicated by yellow. The magnification is 120x.

Figure 8: Image sequence from high-speed fluorescence microscopy. (**A**) Successful delivery of fluorescently labeled nanoparticles of a nanoparticle-and-protein-stabilized microbubble insonified at an ultrasound frequency of 2 MHz and an acoustic pressure amplitude of 600 kPa. (**B**) Unsuccessful delivery of fluorescently labeled nanoparticles of a nanoparticle-and-protein-stabilized microbubble insonified at an ultrasound frequency of 2 MHz and an acoustic pressure amplitude of 210 kPa. Scale bars = 10 µm. The magnification is 120x.

Figure 9: Intravital microscopy after insonation of nanoparticle-and-protein-stabilized microbubbles at an ultrasound frequency of 1 MHz and an acoustic pressure amplitude of 800 kPa. (**A**) Nanoparticles within the vessel, and (**B**) an image sequence of the area indicated by the white dashed square in (**A**) depicting the extravasation of dextran (green) and nanoparticles (red). Scale bars = 50 µm. The magnification is 20x.

DISCUSSION:

Different optical microscopy methods were combined to obtain information on the various steps in the delivery of nanoparticles from the surface of microbubbles to the surrounding medium. Imaging of the bubble oscillations was performed, as well as imaging of the release of the nanoparticles from the bubble shell, the extravasation, and the penetration through the extracellular matrix of tumors *in vivo*. *In vitro* imaging enables screening of many ultrasound parameters compared to the more complex *in vivo* setups. The benefit of combining this range of imaging modalities is the complementary information that can be obtained at different timescales—a feature that is crucial to characterize and optimize the microbubbles for successful delivery and to obtain therapeutic efficacy. This approach is useful to understand the delivery mechanisms for all microbubbles alike, including constructs with fluorescently labeled nanoparticles and drugs.

The most critical steps in the microscopy methods used to study single microbubbles are as follows. For fluorescence microscopy, the nanoparticles should be fluorescently labeled to enable visualization of the particle release. Furthermore, the sample solution should be diluted enough to isolate single microbubbles for analysis in confocal, bright-field, and fluorescence microscopy methods. In addition, it is important to choose an ultrasound driving frequency and acoustic pressure to excite the bubbles most efficiently, namely at their resonance. If the research question concerns delivery of the nanoparticle payload, the appropriate ultrasound parameters should be part of the investigation. Next to resonance, these bubbles should also be driven at or beyond their threshold for nanoparticle release, typically at relatively high acoustic pressure amplitudes (MI > 0.3)[51]. For bright-field microscopy imaging, it is critical to choose a high-speed camera with a sufficiently high framerate to minimize motion blur and to avoid aliasing.

Bright-field microscopy is mainly limited by the imaging framerate and intensity of light sources available, as a higher framerate would give a more detailed time-resolved insight into the bubble

dynamics, but requires more intense illumination. To study particle release in more detail, the framerate for fluorescence imaging can, in principle, be increased by increasing the intensity of the laser light. However, absorption of the high-intensity laser light by the fluorescently labeled microbubbles generates heat, even with high quantum yield dyes. This heat can interfere with the experiments at stake, and in extreme cases, induce photo-thermal cavitation[52]. Thus, in practice, there is a limit to the applied laser intensity. However, intense laser illumination can also be deliberately used to induce particle release from liposomes[53]. Temperature influences bubble dynamics and ultrasound response, depending on bubble type[54]. Therefore, if *in vitro* and intravital methods are to be compared objectively, the *in vitro* methods discussed in the protocol should be performed at 37 °C.

Another limitation of the *in vitro* methods discussed in the current paper is that the bubbles are not in a free-field environment, as microbubbles will rest on the sample holder membrane. Furthermore, there is a selection bias when imaging single microbubbles. However, performing repeated experiments on single bubbles allows for the investigation of the effect of size and removal of the confounding factor—the size distribution. If the bubble response as a function of size can be understood while the concentration is not too high to prevent bubble-bubble interactions, the response of any arbitrary bubble population can be calculated. Finally, both bright-field and fluorescence microscopy methods provide insight into microbubbles convoluted in a two-dimensional (2D) image. If the research question requires more than 2D imaging, the 3D behavior of the bubbles can be resolved by combining the setup described in the protocol with a sideview setup for multiplane imaging[55].

An alternative method to study microbubbles is acoustic characterization[56]. However, measuring the echo of a single microbubble requires locating and isolating a single microbubble within the ultrasound beam[56], which poses a challenge typically tackled by the use of a narrow tube or optical or acoustical tweezers[57,58]. To size bubbles acoustically, the microbubbles can be insonified at frequencies much higher than their resonance frequency, which does not induce volumetric microbubble oscillations[59]. The use of an "acoustical camera" is such a method to image the radial dynamics of single microbubbles in response to ultrasound, wherein a high frequency ultrasound probe is used to determine the radial response of the bubble to a low-frequency driving wave[60]. The disadvantage of this method is that it can only be used to determine the relative change of the microbubble radius; hence, another method is needed to determine the absolute bubble radius, *e.g.*, optical imaging[61,62].

The disadvantage of methods wherein microbubbles are exposed to ultrasound at frequencies higher than their resonance frequency is that at such high frequencies, the penetration depth is decreased[59], limiting the usability for *in vivo* applications. Other forms of microscopy may also be used to study microbubbles such as scanning electron microscopy, atomic force microscopy, and transmission electron microscopy[63]. The achievable spatio-temporal resolution of these alternative microscopy techniques, however, is generally more limited, and these techniques have the disadvantage that imaging is performed either before or after ultrasound exposure by off-line analysis and typically present a low throughput[63]. Another alternative is to use a light scattering method, which can be used to study radial dynamics of single microbubbles in real-

time, but has a low signal to noise ratio as compared to acoustic scattering methods[64].

Real-time intravital microscopy during ultrasound exposure is a powerful method to acquire new insight on the vasculature, behavior of microbubbles, nanoparticles, or other molecules (such as dextran in this case) during ultrasound exposure. A general limitation when performing real-time intravital microscopy is that only a small area of the tissue is imaged, and the penetration depth of the light into tissue is limited. If the imaged vessels contain very few microbubbles and/or nanoparticles within the field of view, little or no information on the nanoparticle behavior and extravasation can be obtained. In addition, because of the limited field of view, a proper alignment between the light and sound paths is crucial. If the ultrasound pressure is high enough to induce bubble destruction, it is also important to choose a pulse repetition frequency that allows fresh bubbles to reperfuse into the field of view between ultrasound pulses. Moreover, as the ultrasound will be reflected from the cover glass in the window chamber and the objective, placing the transducer at an angle is important to reduce reflections to prevent the formation of standing waves, which distort the calibrated pressure field.

Another practical issue is that the setup needs to have enough space to mount the ultrasound transducer and waveguide above or below the objective in the microscope setup. The tumors in the dorsal window chamber will have a limited thickness due to the chamber and the cover slip; however, if needed, other models could be used. Examples are skinfold tumors, for instance, in the mammary fat pad[65] or abdominal intravital imaging of tumors in the various organs[66]. Such tumors can be grown orthotopically in the appropriate microenvironment, and as such, present a more clinically relevant case. The methods described in this work enlighten the potential of fluorescently labeled microbubbles to study the fundamentals of drug delivery applications using bubbles and ultrasound. This combination of microscopy methods provides valuable insight into the microbubble response to ultrasound insonation and its associated acoustic parameter space and presents a clear view of the microbubble and payload behavior over a relevant range of time and length scales.

DISCLOSURES:
The authors declare there is no conflict of interest.

REFERENCES:

1. Szabo, T. L. *Diagnostic ultrasound imaging: inside out*. Academic Press (2004).
2. Paefgen, V., Doleschel, D., Kiessling, F. Evolution of contrast agents for ultrasound imaging and ultrasound-mediated drug delivery. *Frontiers in Pharmacology*. **6**, 197 (2015).
3. Versluis, M., Stride, E., Lajoinie, G., Dollet, B., Segers, T. Ultrasound contrast agents modeling. *Ultrasound in Medicine and Biology*. **46** (9), 2117–2144 (2020).
4. Coelho-Filho, O. R., Rickers, C., Kwong, R. Y., Jerosch-Herold, M. MR myocardial perfusion imaging. *Radiology*. **266** (3), 701–715 (2013).
5. Pandharipande, P. V., Krinsky, G. A., Rusinek, H., Lee, V. S. Perfusion imaging of the liver: current challenges and future goals. *Radiology*. **234** (3), 661–673 (2005).
6. Weidner, N., Carroll, P. R., Flax, J., Blumenfeld, W., Folkman, J. Tumor angiogenesis correlates with metastasis in invasive prostate carcinoma. *The American Journal of Pathology*.

143 (2), 401–409 (1993).
7. Quaia, E. Classification and safety of microbubble-based contrast agents. *Contrast Media in Ultrasonography*. *Medical Radiology (Diagnostic Imaging).* Quaia, E. (Ed), Springer, Berlin, Heidelberg, 3–14 (2005).
8. Unger, E. C., Porter, T., Culp, W., Labell, R., Matsunaga, T., Zutshi, R. Therapeutic applications of lipid-coated microbubbles. *Advanced Drug Delivery Reviews*. **56** (9), 1291–1314 (2004).
9. Blomley, M. J. K., Cooke, J. C., Unger, E. C., Monaghan, M. J., Cosgrove, D. O. Microbubble contrast agents: a new era in ultrasound. *BMJ*. **322** (7296), 1222–1225 (2001).
10. Faez, T. et al. 20 years of ultrasound contrast agent modeling. *IEEE transactions on ultrasonics, ferroelectrics, and frequency control*. **60** (1), 7–20 (2012).
11. De Jong, N., Emmer, M., Van Wamel, A., Versluis, M. Ultrasonic characterization of ultrasound contrast agents. *Medical & Biological Engineering & Computing*. **47** (8), 861–873 (2009).
12. De Jong, N. Acoustic properties of ultrasound contrast agents (1993).
13. Schneider, M. Characteristics of sonovue™. *Echocardiography*. **16**, 743–746 (1999).
14. Klibanov, A. L. Microbubble contrast agents: targeted ultrasound imaging and ultrasound-assisted drug-delivery applications. *Investigative Radiology*. **41** (3), 354–362 (2006).
15. Averkiou, M. A., Powers, J., Skyba, D., Bruce, M., Jensen, S. Ultrasound contrast imaging research. *Ultrasound Quarterly*. **19** (1), 27–37 (2003).
16. Snipstad, S. et al. Contact-mediated intracellular delivery of hydrophobic drugs from polymeric nanoparticles. *Cancer Nanotechnology*. **5** (1), 8 (2014).
17. Epstein, P. S., Plesset, M. S. On the stability of gas bubbles in liquid-gas solutions. *The Journal of Chemical Physics*. **18** (11), 1505–1509 (1950).
18. Borden, M. A., Longo, M. L. Dissolution behavior of lipid monolayer-coated, air-filled microbubbles: effect of lipid hydrophobic chain length. *Langmuir*. **18** (24), 9225–9233 (2002).
19. Deshpande, N., Needles, A., Willmann, J. K. Molecular ultrasound imaging: current status and future directions. *Clinical Radiology*. **65** (7), 567–581 (2010).
20. Miller, M. W., Miller, D. L., Brayman, A. A. A review of in vitro bioeffects of inertial ultrasonic cavitation from a mechanistic perspective. *Ultrasound in Medicine & Biology*. **22** (9), 1131–1154 (1996).
21. Snipstad, S. et al. Sonopermeation to improve drug delivery to tumors: from fundamental understanding to clinical translation. *Expert Opinion on Drug Delivery*. **15** (12), 1249–1261 (2018).
22. Dimcevski, G. et al. A human clinical trial using ultrasound and microbubbles to enhance gemcitabine treatment of inoperable pancreatic cancer. *Journal of Controlled Release*. **243**, 172–181 (2016).
23. May, J. -N. et al. Multimodal and multiscale optical imaging of nanomedicine delivery across the blood-brain barrier upon sonopermeation. *Theranostics*. **10** (4), 1948–1959 (2020).
24. Carmen, J. C. et al. Ultrasonic-enhanced gentamicin transport through colony biofilms of *Pseudomonas aeruginosa* and *Escherichia coli*. *Journal of Infection and Chemotherapy*. **10** (4), 193–199 (2004).
25. Runyan, C. M. et al. Low-frequency ultrasound increases outer membrane permeability of *Pseudomonas aeruginosa*. *The Journal of General and Applied Microbiology*. **52** (5), 295–301 (2006).

26. Yemane, P. T. et al. Effect of ultrasound on the vasculature and extravasation of nanoscale particles imaged in real time. *Ultrasound in Medicine & Biology*. **45** (11), 3028–3041 (2019).
27. van Wamel, A. et al. Acoustic Cluster Therapy (ACT) enhances the therapeutic efficacy of paclitaxel and Abraxane® for treatment of human prostate adenocarcinoma in mice. *Journal of Controlled Release*. **236**, 15–21 (2016).
28. Snipstad, S. et al. Ultrasound improves the delivery and therapeutic effect of nanoparticle-stabilized microbubbles in breast cancer xenografts. *Ultrasound in Medicine & Biology*. **43** (11), 2651–2669 (2017).
29. Sheikov, N., McDannold, N., Vykhodtseva, N., Jolesz, F., Hynynen, K. Cellular mechanisms of the blood-brain barrier opening induced by ultrasound in presence of microbubbles. *Ultrasound in Medicine & Biology*. **30** (7), 979–989 (2004).
30. Hynynen, K., McDannold, N., Sheikov, N. A., Jolesz, F. A., Vykhodtseva, N. Local and reversible blood–brain barrier disruption by noninvasive focused ultrasound at frequencies suitable for trans-skull sonications. *Neuroimage*. **24** (1), 12–20 (2005).
31. Åslund, A. K. O. et al. Nanoparticle delivery to the brain—By focused ultrasound and self-assembled nanoparticle-stabilized microbubbles. *Journal of Controlled Release*. **220**, 287–294 (2015).
32. Downs, M. E., Buch, A., Karakatsani, M., Konofagou, E. E., Ferrera, V. P. Blood-brain barrier opening in behaving non-human primates via focused ultrasound with systemically administered microbubbles. *Scientific Reports*. **5**, 15076 (2015).
33. Baghirov, H. et al. Ultrasound-mediated delivery and distribution of polymeric nanoparticles in the normal brain parenchyma of a metastatic brain tumour model. *PloS One*. **13** (1), e0191102 (2018).
34. Sulheim, E. et al. Therapeutic effect of cabazitaxel and blood-brain barrier opening in a patient-derived glioblastoma model. *Nanotheranostics*. **3** (1), 103 (2019).
35. Lentacker, I. et al. Lipoplex-loaded microbubbles for gene delivery: a Trojan Horse controlled by ultrasound. *Advanced Functional Materials*. **17** (12), 1910–1916 (2007).
36. De Temmerman, M. et al. mRNA-Lipoplex loaded microbubble contrast agents for ultrasound-assisted transfection of dendritic cells. *Biomaterials*. **32** (34), 9128–9135 (2011).
37. Burke, C. W., Alexander, E., Timbie, K., Kilbanov, A. L., Price, R. J. Ultrasound-activated agents comprised of 5FU-bearing nanoparticles bonded to microbubbles inhibit solid tumor growth and improve survival. *Molecular Therapy*. **22** (2), 321–328 (2014).
38. Mørch, Ý. et al. Nanoparticle-stabilized microbubbles for multimodal imaging and drug delivery. *Contrast Media & Molecular Imaging*. **10** (5), 356–366 (2015).
39. Jamburidze, A. et al. Nanoparticle-coated microbubbles for combined ultrasound imaging and drug delivery. *Langmuir*. **35** (31), 10087–10096 (2019).
40. Snipstad, S. et al. Sonopermeation enhances uptake and therapeutic effect of free and encapsulated cabazitaxel. *Ultrasound in Medicine and Biology*. doi: https://doi.org/10.1016/j.ultrasmedbio.2020.12.026 (2021).
41. De Cock, I., Lajoinie, G., Versluis, M., De Smedt, S. C., Lentacker, I. Sonoprinting and the importance of microbubble loading for the ultrasound mediated cellular delivery of nanoparticles. *Biomaterials*. **83**, 294–307 (2016).
42. Roovers, S. et al. Sonoprinting of nanoparticle-loaded microbubbles: Unraveling the multi-timescale mechanism. *Biomaterials*. **217**, 119250 (2019).

43. Klymchenko, A. S. et al. Highly lipophilic fluorescent dyes in nano-emulsions: towards bright non-leaking nano-droplets. *RSC Advances*. **2** (31), 11876 (2012).
44. Åslund, A. K. O. et al. Quantification and qualitative effects of different PEGylations on Poly (butyl cyanoacrylate) Nanoparticles. *Molecular Pharmaceutics*. **14** (8), 2560–2569 (2017).
45. Born, M., Wolf, E. *Principles of optics: electromagnetic theory of propagation, interference and diffraction of light*. Cambridge University Press, Cambridge; New York (1999).
46. Pittet, M. J., Weissleder, R. Intravital imaging. *Cell*. **147** (5), 983–991 (2011).
47. Hak, S., Reitan, N. K., Haraldseth, O., de Lange Davies, C. Intravital microscopy in window chambers: a unique tool to study tumor angiogenesis and delivery of nanoparticles. *Angiogenesis*. **13** (2), 113–130 (2010).
48. Fusser, M. et al. Cabazitaxel-loaded Poly (2-ethylbutyl cyanoacrylate) nanoparticles improve treatment efficacy in a patient derived breast cancer xenograft. *Journal of Controlled Release*. **293**, 183–192 (2019).
49. Abou-Saleh, R. H. et al. Molecular effects of glycerol on lipid monolayers at the gas–liquid interface: impact on microbubble physical and mechanical properties. *Langmuir*. **35** (31), 10097–10105 (2019).
50. Seynhaeve, A. L. B., ten Hagen, T. L. M. Intravital microscopy of tumor-associated vasculature using advanced dorsal skinfold window chambers on transgenic fluorescent mice. *Journal of Visualized Experiments*. (131), 55115 (2018).
51. Luan, Y. et al. Lipid shedding from single oscillating microbubbles. *Ultrasound in Medicine & Biology*. **40** (8), 1834–1846 (2014).
52. Lajoinie, G. et al. Ultrafast vapourization dynamics of laser-activated polymeric microcapsules. *Nature Communications*. **5** (1), 1–8 (2014).
53. Mathiyazhakan, M. et al. Non-invasive controlled release from gold nanoparticle integrated photo-responsive liposomes through pulse laser induced microbubble cavitation. *Colloids and Surfaces B: Biointerfaces*. **126**, 569–574 (2015).
54. Vos, H. J., Emmer, M., de Jong, N. Oscillation of single microbubbles at room versus body temperature. *2008 IEEE Ultrasonics Symposium*. 982–984, doi: 10.1109/ULTSYM.2008.0237 (2008).
55. Vos, H. J., Dollet, B., Bosch, J. G., Versluis, M., de Jong, N. Nonspherical vibrations of microbubbles in contact with a wall—a pilot study at low mechanical index. *Ultrasound in Medicine & Biology*. **34** (4), 685–688 (2008).
56. Sijl, J. et al. Acoustic characterization of single ultrasound contrast agent microbubbles. *The Journal of the Acoustical Society of America*. **124** (6), 4091–4097 (2008).
57. Garbin, V. et al. Changes in microbubble dynamics near a boundary revealed by combined optical micromanipulation and high-speed imaging. *Applied Physics Letters*. **90** (11), 114103 (2007).
58. Baresch, D., Garbin, V. Acoustic trapping of microbubbles in complex environments and controlled payload release. *Proceedings of the National Academy of Sciences of the United States of America*. **117** (27), 15490–15496 (2020).
59. Maresca, D. et al. Acoustic sizing of an ultrasound contrast agent. *Ultrasound in Medicine & Biology*. **36** (10), 1713–1721 (2010).
60. Renaud, G., Bosch, J. G., van der Steen, A. F. W., de Jong, N. An "acoustical camera" for *in vitro* characterization of contrast agent microbubble vibrations. *Applied Physics Letters*. **100** (10),

101911 (2012).
61. Renaud, G., Bosch, J. G., Van Der Steen, A. F. W., De Jong, N. Low-amplitude non-linear volume vibrations of single microbubbles measured with an “acoustical camera.” *Ultrasound in Medicine & Biology*. **40** (6), 1282–1295 (2014).
62. Luan, Y. et al. Combined optical sizing and acoustical characterization of single freely-floating microbubbles. *Applied Physics Letters*. **109** (23) (2016).
63. Lajoinie, G. et al. *In vitro* methods to study bubble-cell interactions: Fundamentals and therapeutic applications. *Biomicrofluidics*. **10** (1), 011501 (2016).
64. Guan, J., Matula, T. J. Using light scattering to measure the response of individual ultrasound contrast microbubbles subjected to pulsed ultrasound *in vitro*. *The Journal of the Acoustical Society of America*. **116** (5), 2832–2842 (2004).
65. Sofias, A. M., Åslund, A. K. O., Hagen, N., Grendstad, K., Hak, S. Simple and robust intravital microscopy procedures in hybrid TIE2GFP-BALB/c transgenic mice. *Molecular Imaging and Biology*. **22** (3), 486–493 (2020).
66. Ritsma, L., Steller, E. J. A., Ellenbroek, S .I. J., Kranenburg, O., Borel Rinkes, I. H. M., van Rheenen, J. Surgical implantation of an abdominal imaging window for intravital microscopy. *Nature Protocols*. **8** (3), 583–594 (2013).

Figure 1

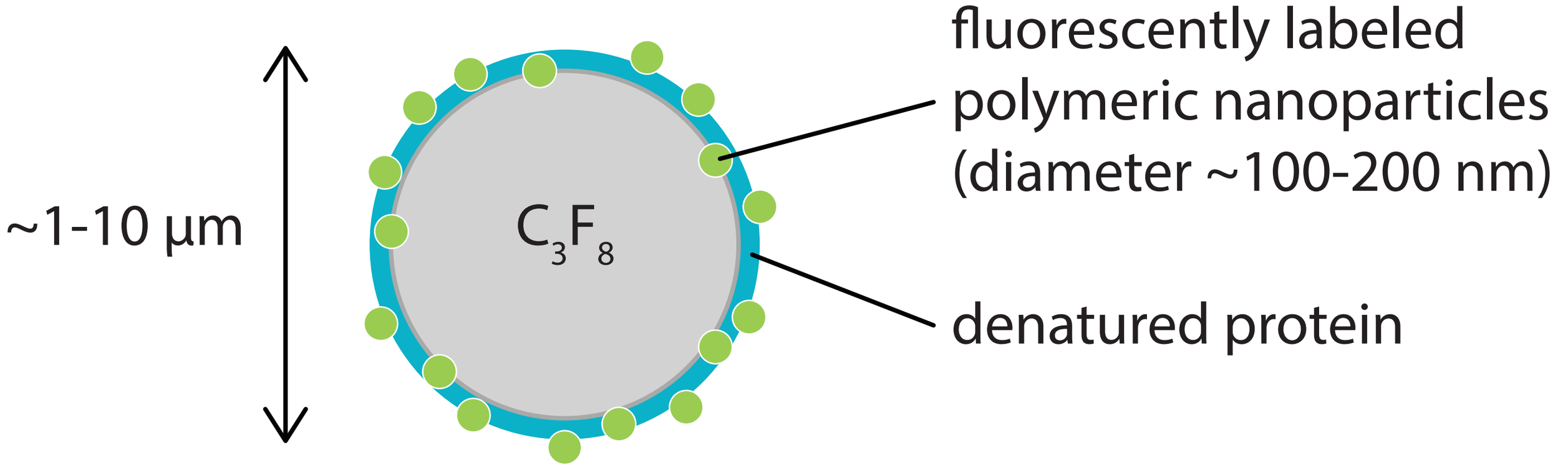

Figure 2

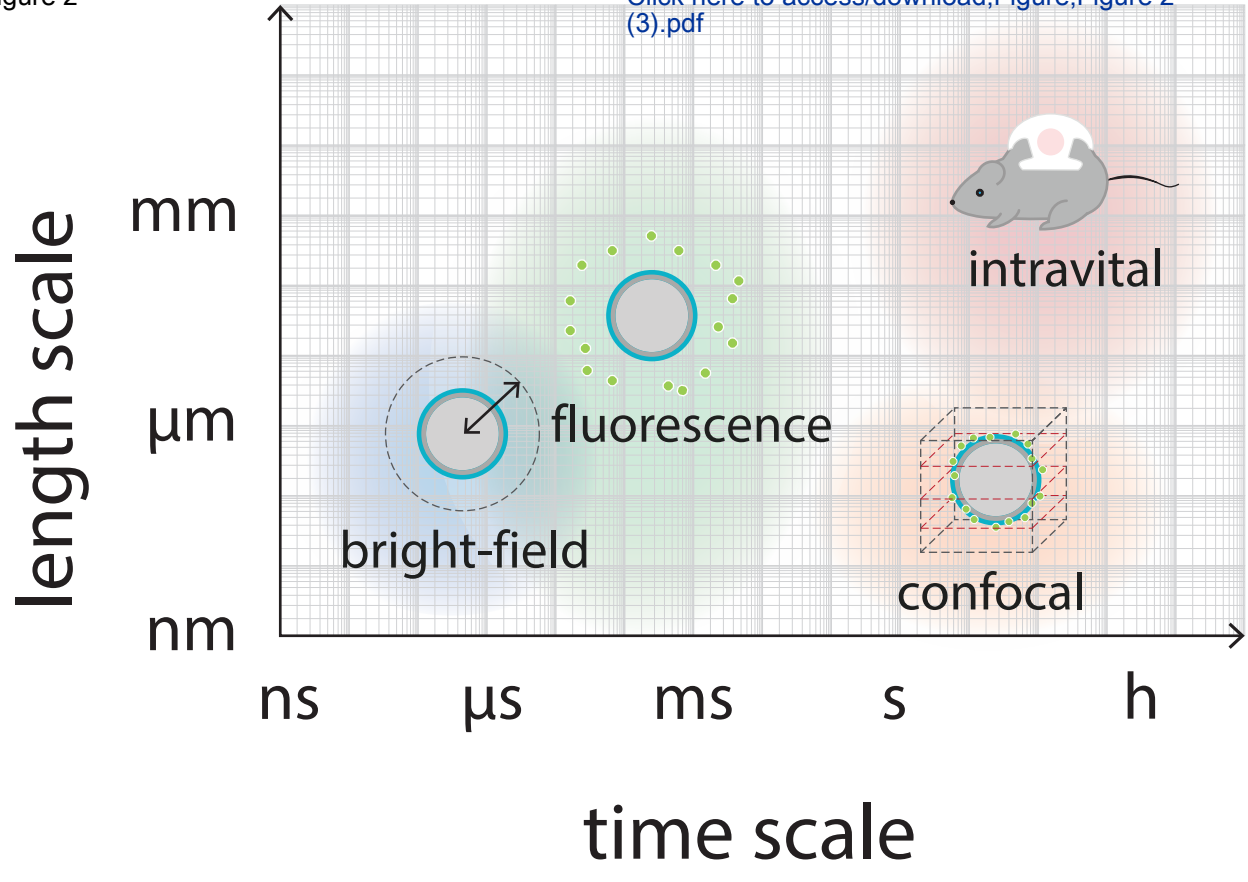

Figure 3

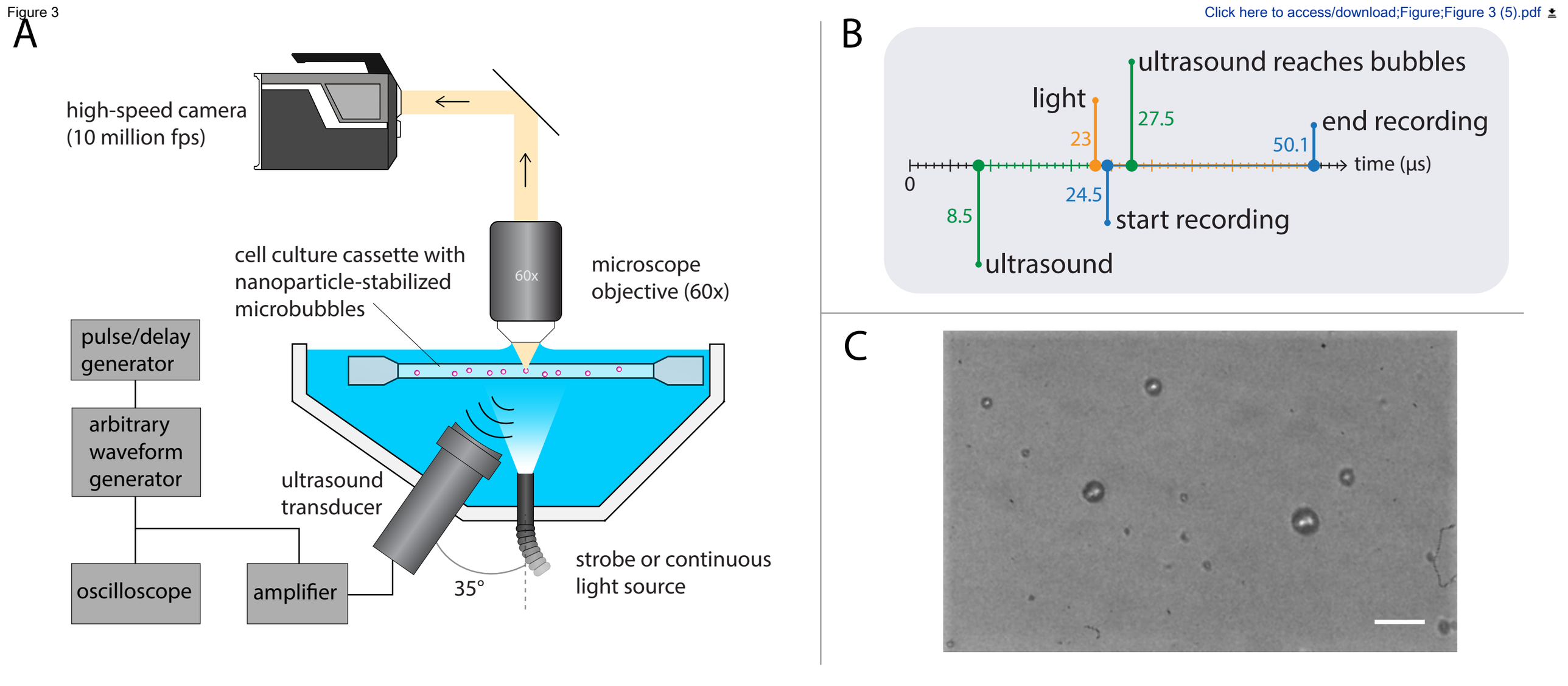

Figure 4

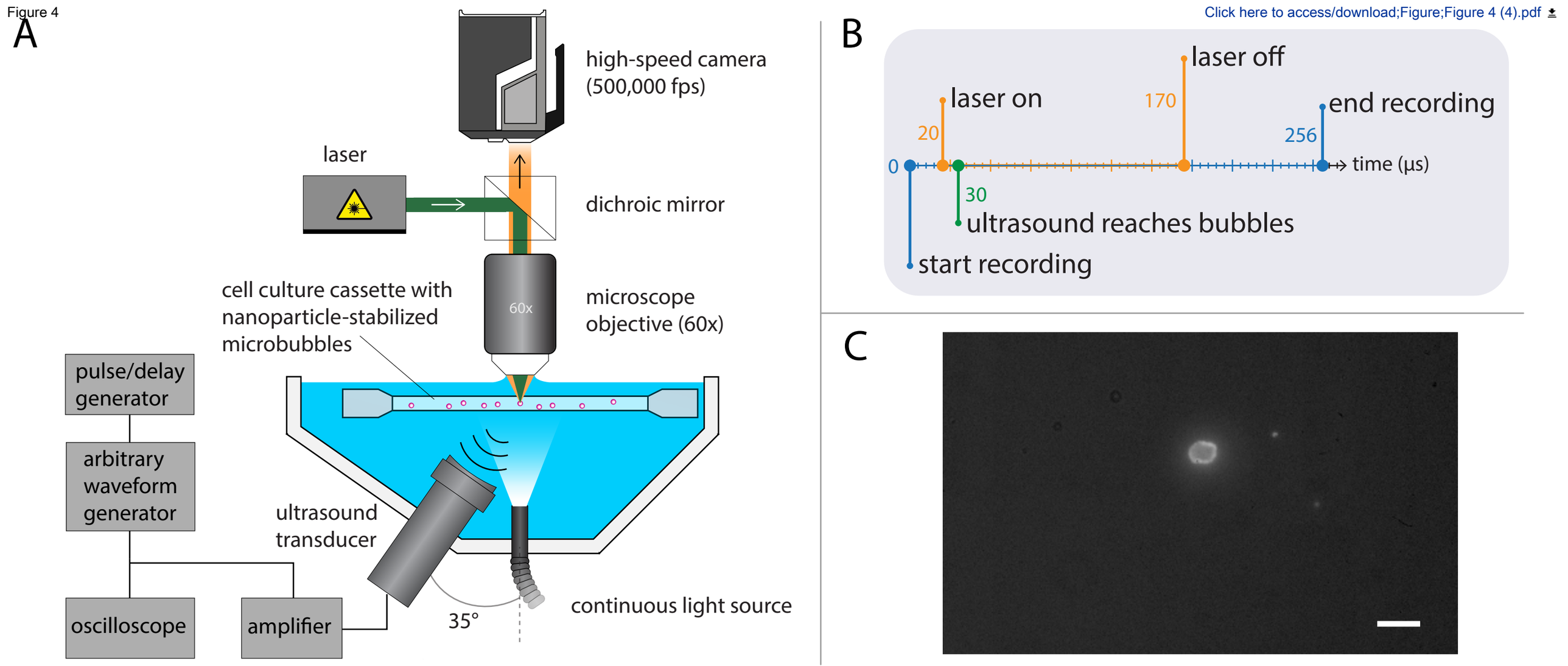

Figure 5

A

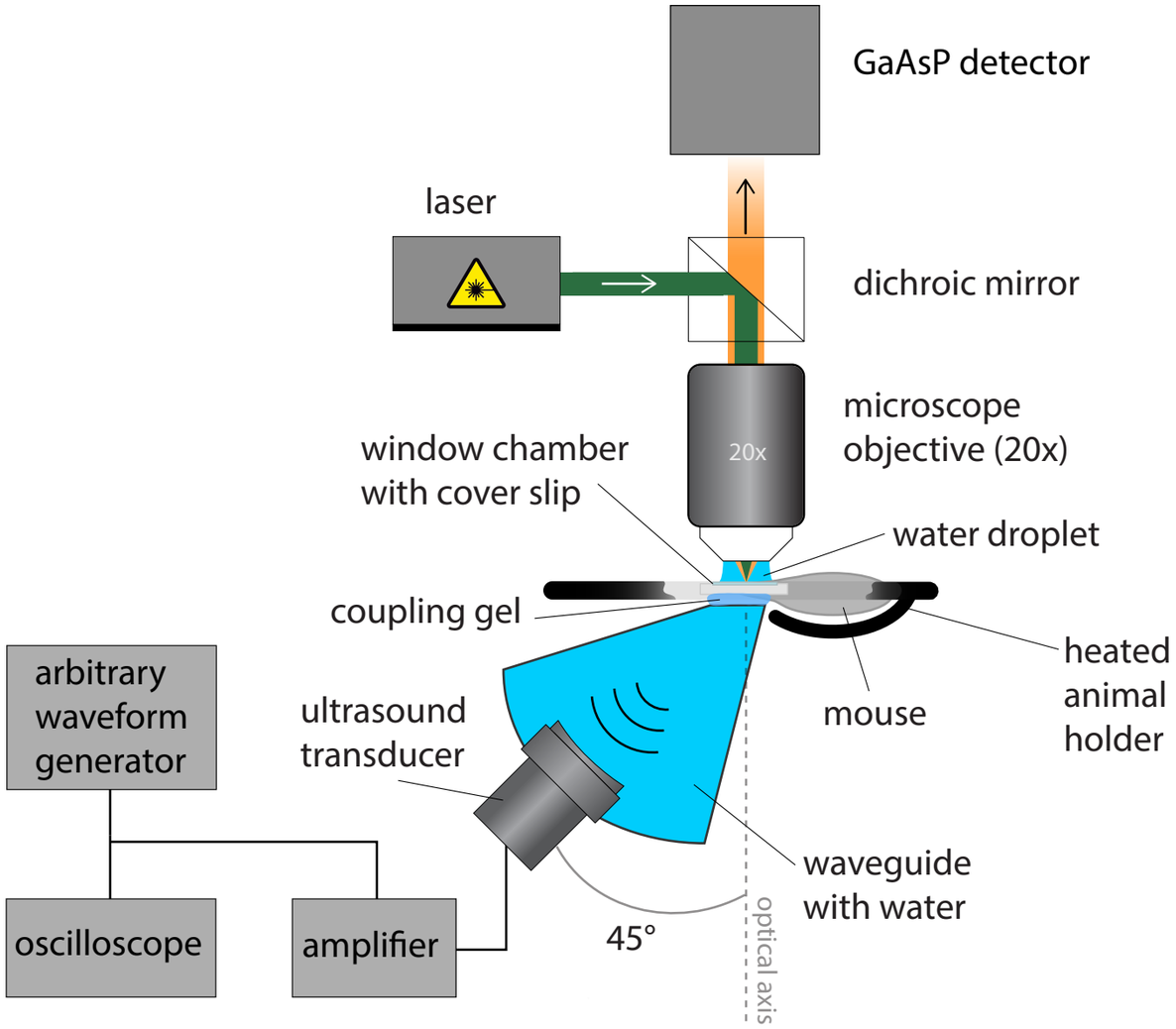

B

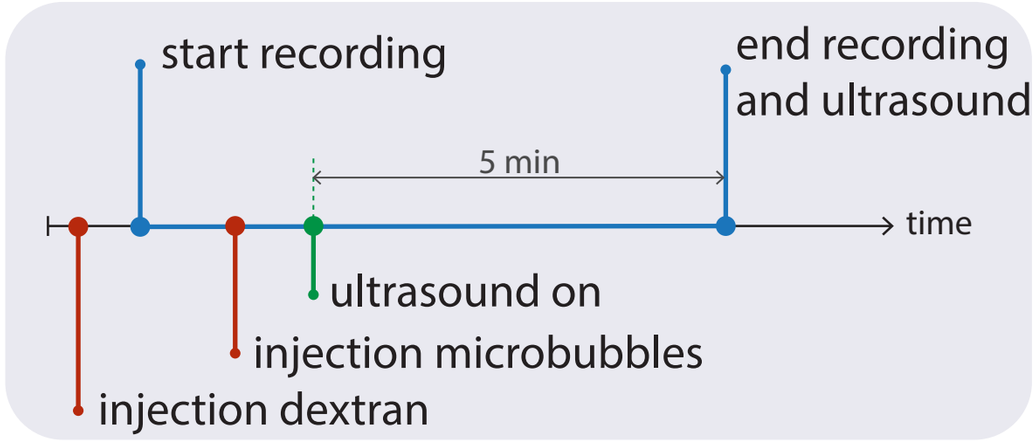

C

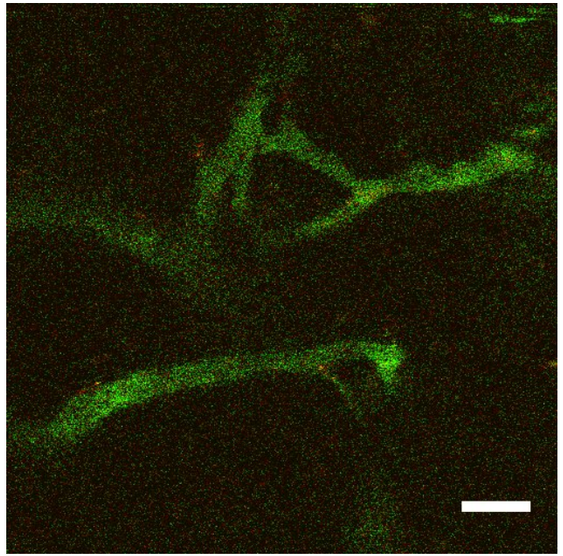

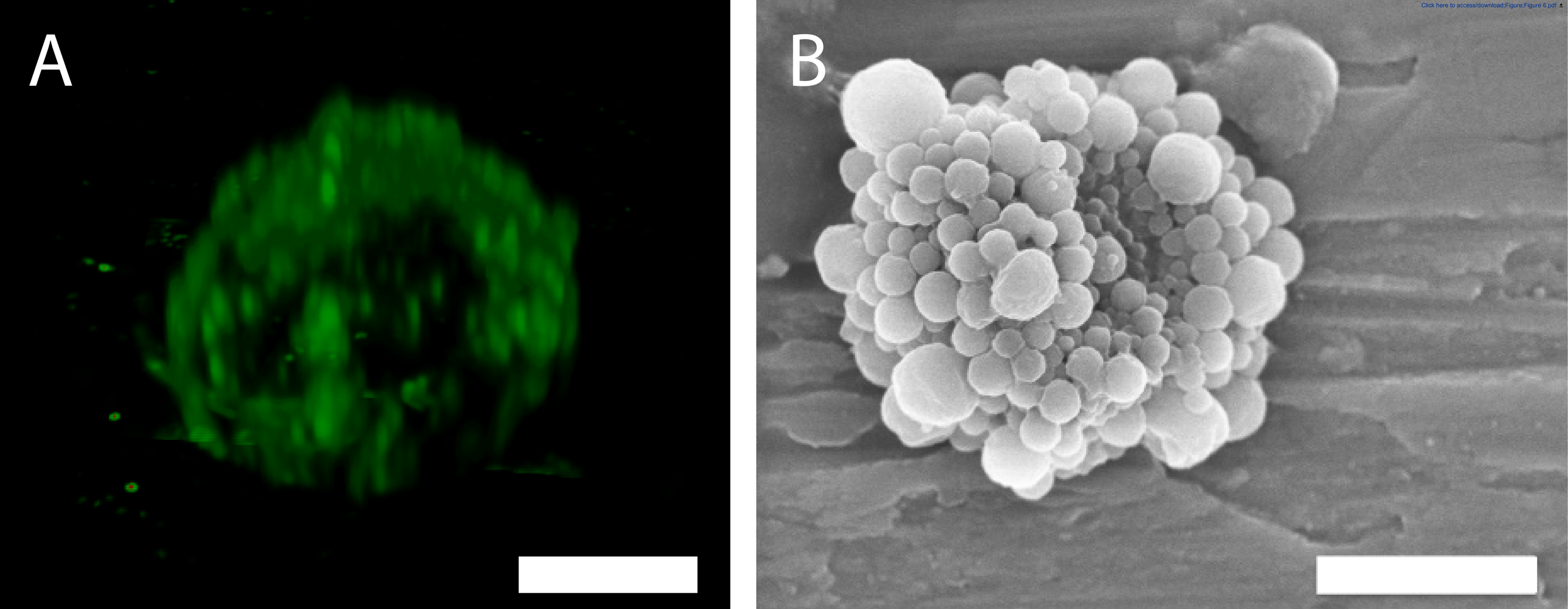

Figure 7

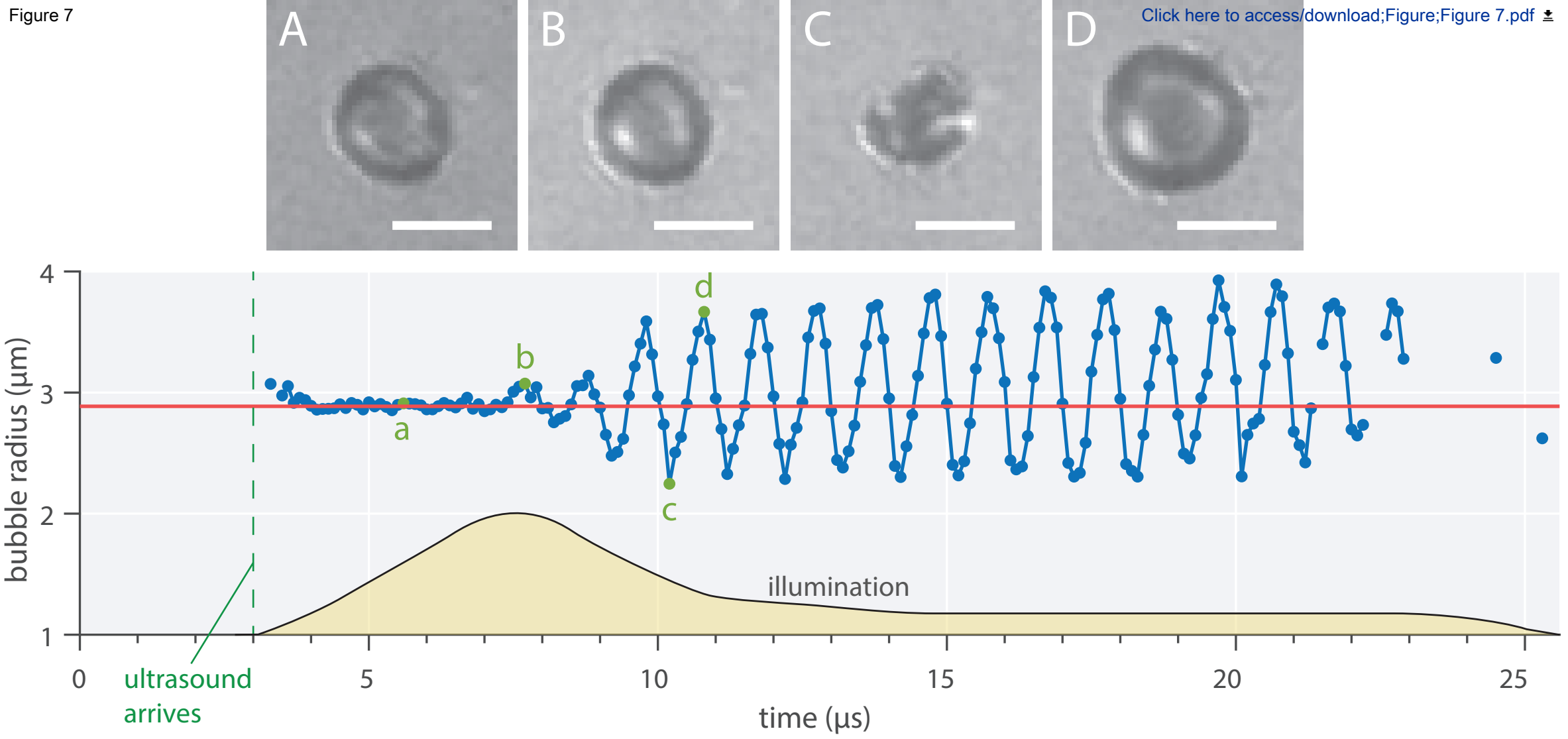

Figure 8

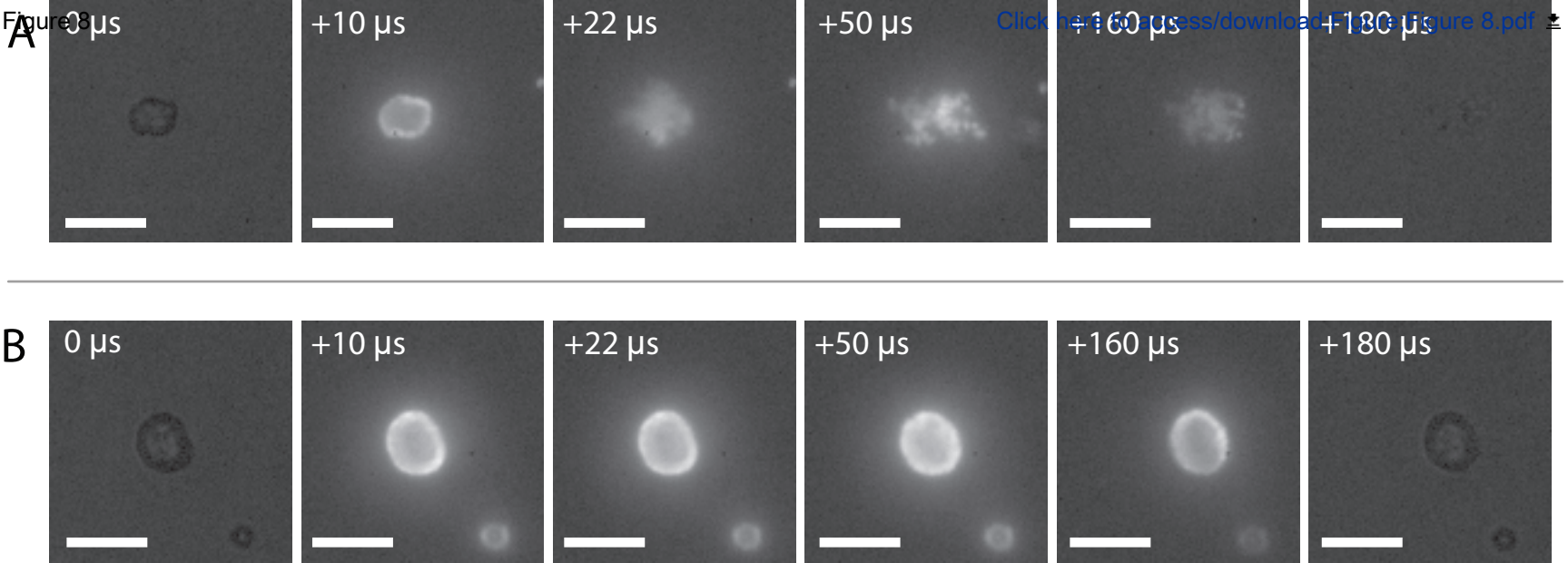

Figure 9

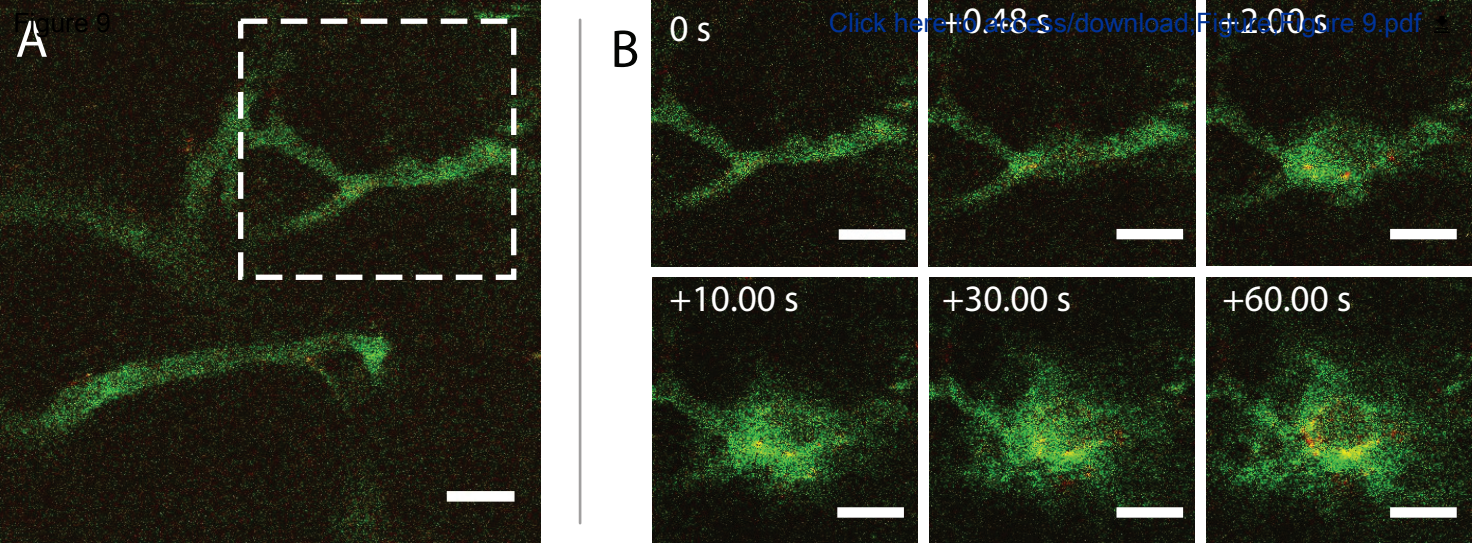

Name of Material/Equipment	Company	Catalog Number
100 MS/s Dual-Channel Arbitrary Waveform Generator model 8026	Tabor Electronics	
2100 L	ENI	
2 MDa dextran	Sigma-Aldrich	
33522 A	Agilent Technologies	
A1R	Nikon Instruments	
ACE I	SCHOTT	
Atipemazol	Orion Pharma	
Baytril	Bayer	
BD Neoflon 24 G	Becton Dickinson & Company	
BNC model 575	Berkely Nucleonics Corporation	
Branson 2510 Ultrasonic Cleaner	Branson	
Channel slide	Ibidi	
CLINIcell 25	Laboratoires Mabio International	
Cohlibri	Lightline	
DP03014 Digital Phosphor Oscilloscope	Tektronix	
Fentanyl	Actavis Group HF	
Fetal Bovine Serum	Sigma-Aldrich	
Fiber-optic hydrophone	Precision Acoustics	
Flumanezil	Fresenius Kabi	
Heated animal holder	Custom design	
Hyper Vision HPV-X2	Shimadzu	
ImageJ	National Institutes of Health and the Laboratory for Optical and Computational Instrumentation, University of Wisconsin	
In vivo SliceScope	Scientifica	
Isoflurane	Baxter	
ISOTON	Beckman Coulter	
LUMPLFLN60XW	Olympus	
MaiTai DeepSee	Spectra-Physics	

MATLAB	Mathworks
Medetomidine	Orion Pharma
Midazolam	Accord Healthcare Limited
Milli-Q	Merck
MVS 7010 High Intensity Xenon Strobe	PerkinElmer
Panametrics-NDT C305	Olympus
Panametrics-NDT V304	Olympus
Penicillin	Sigma-Aldrich
Perfluoropropane gas	F2 Chemicals
Roswell Park Memorial Institute 1640	Gibco Thermo-Fisher
Safe-Lock tube	Eppendorf
Streptomycin	Sigma-Aldrich
T 25 basic ULTRA-TURRAX	IKA laboratory technology
TDS 210	Tektronix
Transducer	Precision Acoustics Ltd
U-TLU	Olympus
VBA100-200	Vectawave
Window chambers	Custom made
XLUMPLFLN20 XW	Olympus
XY(Z) translation stages	Thorlabs

Comments/Description

Arbitrary waveform generator (programmable)
Amplifier, used in window chamber setup

Arbitrary wave form generator, used in window chamber setup
Confocal microscope
Dimmable AC halogen light source
Antidote to wake animal
Enrofloxacin
Tail vein catheter
Pulse/delay generator
Ultrasonic bath

Cell culture casette (volume 10 mL, membrane area 25 cm^2, membrane thickness 175 µm)
Laser (5 W, excitation wavelength 532 nm)
Oscilloscope
Anaesthesia of mouse
Supplement for cell culture medium
Used for alignment
Antidote to wake animal
A steel holder where the mouse is positioned on its side in a cavity fitting the size of a mouse, with the window chamber lying flat anc
High-speed camera

open source image processing program
Multiphoton microscope

Filtered, phosphate-buffered saline solution
Water immersion objective (magnification 60x, working distance 2 mm)
Pulsed laser

Programming environment
Anesthesia of mouse
Anesthesia of mouse
Ultrapure water
Strobe light
Single-element focused immersion transducer (center frequency 2.25 MHz, focal distance 1", diameter 1")
Single-element focused immersion transducer (center frequency 2.25 MHz, focal distance 1.88", diameter 1.25")
Addition to cell culture medium before implantation of tumor in animals

Cell culture medium

Addition to cell culture medium before implantation of tumor in animals
Dispersion tool
Oscilloscope, used in window chamber setup
Used in window chamber setup
Tube lens
Amplifier
Used in window chamber setup
20x water dipping objective

d immobilized with screws on each side. Below the chamber there is a hole in the holder to secure acoustic contact between the trans

sducer and the skin. The holder is heated to a maximum temperature of 37°C, and the temperature is controlled by feedback from a

rectal temperature probe in the mouse. The holder is mounted to an XY positioning stage so the animal can be moved independently

' to image different areas of the window chamber

Manuscript JoVE62251: editorial and peer review

Editorial comments:

1. Please take this opportunity to thoroughly proofread the manuscript to ensure that there are no spelling or grammar issues.

The manuscript was once again proofread for spelling and grammatical errors and these are now corrected.

2. Please revise the following lines to avoid previously published work: 62-63, 109-110, 515-516, 591-593, 600-603.

Lines 62-63 were approved by the editor.

Lines 109-110 have been rephrased to avoid overlap with reference [1]. It has been changed from "[…] increase the permeability of the blood-brain barrier, allowing therapeutic agents to enter the brain parenchyma" to: "increase the blood-brain barrier permeability, enabling drugs to enter the brain parenchyma".

Lines 515-516 have been rewritten to avoid overlap with reference [2]. It has been changed from "[…] positioned below the objective at an angle of 45° with respect to the optical axis to minimize reflections from the glass of the window chamber and reduce standing wave formations" to "[…] positioned below the objective at an angle of 45° with respect to the optical axis to minimize reflections from the cover glass of the dorsal skinfold window chamber and to reduce standing wave formations".

Lines 591-593 have been revised to avoid overlap with reference [2]. It has been changed from " Multiphoton microscopy was used for real-time intravital imaging during ultrasound to investigate the effects of ultrasound and microbubbles on nanoparticle behavior in the blood, enhancing the permeability of tumor blood vessels and improving the delivery of nanoparticles." to "Real-time intravital multiphoton microscopy during ultrasound was used to investigate the effects of ultrasound and microbubbles on nanoparticle behavior in the blood, enhancement of the permeability of tumor blood vessels and improvement of the delivery of nanoparticles."

Lines 600-603 have been revised to avoid overlap with reference [2]. It has been changed from "Results gained from intravital multiphoton microscopy help to elucidate the temporal and spatial extravasation of nanoscale particles during ultrasound exposure, which is highly beneficial to complete our understanding of the mechanisms underlying ultrasound-mediated delivery of nanoparticles and for optimizing such technologies[2]." to "Results gained from intravital multiphoton microscopy elucidate the spatial and temporal extravasation of nanoparticles during ultrasound exposure, which is highly beneficial to complete the understanding of the mechanisms underlying ultrasound-mediated delivery of nanoparticles and to optimize such technologies[2]"

3. As we are filming in Enschede, Overijssel, Netherlands, please provide the footage of the sections of the protocol from Trondheim here:
https://www.dropbox.com/request/EfnRxOtoNAVNUPbHAqNb

Footage of the sections of the protocol from Trondheim will be uploaded to the Dropbox folder.

4. Please provide an institutional email address for each author.

Institutional email addresses have been added for all authors.

5. Please revise the text to avoid the use of any personal pronouns (e.g., "we", "you", "our" etc.).

The use of personal pronouns has been completely omitted from the manuscript. In line 41-43: “we focus on” has been rephrased to “the focus is on”. In line 652-653: “We imaged the bubble oscillations” is replaced by “Imaging of the bubble oscillations was performed, as well as imaging of”.

in line 146-147: “our systems” has been replaced by “the systems at hand”. In line 600-603: “our understanding” has been changed to “understanding”.

6. JoVE cannot publish manuscripts containing commercial language. This includes trademark symbols (™), registered symbols (®), and company names before an instrument or reagent. Please remove all commercial language from your manuscript and use generic terms instead. All commercial products should be sufficiently referenced in the Table of Materials (Eppendorf, ISOTON, MATLAB, CLINIcell, Shimadzu, Olympus)

“CLINIcell”, “Shimadzu” and “Olympus” were not mentioned in the originally submitted manuscript, but were present in the figures. These words have been replaced by generic terms as mentioned in editorial comment 19.

The word “MATLAB” as was used in step 2.2.7.1 (lines 376-381), step 2.3.6.1 (line 459-462), and step 3.7.1 (line 562-565) is now changed to “programming environment”. In the results (line 578) the word “MATLAB” is now replaced by “a script written in-house”.

“Baytril” as mentioned in step 3.1.6 (line 490-492) has been changed to “enrofloxacin”.

”ImageJ” as mentioned in step 3.7.1 (line 562-565) has been changed to “(open source) image processing software”.

7. Please remove “(Table of Materials)” from the protocol section.

A general statement has been added before the first step of the protocol regarding the Table of Materials: “Details of materials that are used in the protocol can be found in the Table of Materials.” All references to the Table of Materials in the protocol steps have been removed.

8. Line 187: Please convert stirring speeds to centrifugal force (x g) instead of revolutions per minute (rpm).

The diameter of rotation of the dispersion tool is 6.1 mm. A radius of 3 mm and 24,000 rpm then is equivalent to 1935 g. The radius of rotation and the stirring speed in centrifugal force are now added to step 1.4. The stirring speed is also specified in revolutions per minute, as this is the unit of the settings of the particular dispersion tool used in the production of the microbubbles of this paper.

9. Line 192-193: Please specify the temperature in which the excess casein and nanoparticle is stored. What is the concentration of acetone used for cleaning?

Line 192-193 is rephrased to “Store the excess casein and nanoparticle solution at 4°C and clean the dispersion tool with 100% acetone.” to include the temperature at which the excess casein and nanoparticles are stored, and the concentration of acetone used for cleaning.

10. Line 201-203: Please specify the dilution of the bubble solution. What is the size of the venting needle and the glass vial used?

The dilution of the bubble solution is specified in step 2.1.1.3. Steps 2.1.1.1 and 2.1.1.2 merely specify the necessary steps to reach such dilution. The specification of the venting needle size (19G - 21G) has been added to step 2.1.1.1. Additional details of the glass crimp top vial (10 mL, diameter of 2 cm) have been added to step 1.1.

11. Line 206: Please include the amount of bubble solution taken out.

The amount of bubble solution will depend on the type of bubble that is used. In our case, a small syringe was used to extract 0.2 mL of the bubble suspension so that a concentration of approximately 2 x 10^5 to 6 x 10^5 microbubbles/mL could be reached in step 2.1.1.3. This information has been added to step 2.1.1.2.

12. Line 214: Please include the details of the washing steps.

Washing was not performed during the experiments presented in this work, i.e., free nanoparticles remained in suspension. For the present confocal imaging experiments the free nanoparticles did not pose a problem, as free particles are easily distinguished from microbubbles in confocal imaging. However, if washing of the bubbles is required, e.g. for epifluorescence imaging, the produced bubble suspension is to be diluted (e.g. by taking 100 µL of the bubble solution in 10 mL of phosphate buffered saline), after which the diluted suspension is centrifuged (typically at speeds of the order of 100 g). Finally, the supernatant containing the microbubbles can be removed with a pipette for further analysis. The pellet/precipitate then contains the free fluorescent particles and can be disposed. The washing step should be repeated as necessary. A description of this washing process has been added to line 214-216.

For the nanoparticles, freely suspended dye is removed by dialysis after synthesis of the nanoparticles and before the microbubbles are produced. Since this step is very specific to this type of microbubble, this washing step is not included in the protocol.

13. Line 237: Please comment on z-stack imaging? Any specific step size used?

The step size used in the z-direction was 100 nm. This specification has now been added to the manuscript.

14. Line 468-470: Please include an ethics statement before your numbered protocol steps, indicating that the protocol follows the animal care guidelines of your institution. Any age and sex specific bias?

The ethics statement from the Norwegian Animal Research Authorities is now moved to before the numbered protocol steps. There is no age and sex specific bias, but the weight of the mice should meet a criterium for the skin to be suitable. Line 468-470 is rephrased to: “Both female and male mice can be used, and age is unimportant, but the weight of the mice should be at least 22-24 g for the skin to be sufficiently flexible.”

15. Line 496: Please provide the details of the anesthesia? What was the induction dose of isoflurane? How long was the procedure?

The induction and maintenance dose of the anesthesia (line 496) is now specified. It is 5% and 1-2%, respectively. The procedure spans a couple of minutes, which has also been added to step 3.2.1.

16. Line 497-499: Please specify the type of the cancer cells used? Please comment on the cell culture medium. How was the tumor growth ensured?

A line has been added to step 3.2.1 regarding the type of cancer cells: “In the experiments described, the human osteosarcoma (OHS) cell line was used, but other cell lines can also be used.”

The cell culture medium used for tumor model creation is Roswell Park Memorial Institute (RPMI) 1640, supplemented with 10% Fetal Bovine Serum. Before implantation in animals 100 U/mL penicillin and 100 mg/mL streptomycin have been added. These materials are now included in step 3.2.1 and have been added to the Table of Materials.

Prior to implantation, the cells are maintained at 37°C and 5% CO_2. A note on this has now been added after step 3.2.1.

17. Line 533: Please include the specifications of the heated animal holder.

A description of the heated animal holder has been added to the Table of Materials: “A steel holder where the mouse is positioned on its side in a cavity fitting the size of a mouse, with the window chamber lying flat and immobilized with screws on each side. Below the chamber there is a hole in the holder to secure acoustic contact between the transducer and the skin. The holder is heated to a maximum temperature of 37°C, and the temperature is controlled by feedback from a rectal temperature probe in the mouse. The holder is mounted to an XY positioning stage so the animal can be moved independently to image different areas of the window chamber.“

18. Please obtain explicit copyright permission to reuse any figures from a previous publication. Explicit permission can be expressed in the form of a letter from the editor or a link to the editorial policy that allows re-prints. Please upload this information as a .doc or .docx file to your Editorial Manager account. The Figure must be cited appropriately in the Figure Legend, i.e. “This figure has been modified from [citation].”

Figure 6b contains a reproduction of a figure by Sulheim et al., 2019 (reference 34 of the manuscript). It was published in the journal ‘Nanotheranostics’, which states on its website (ntno.org/ms/terms) that: “As an author or co-author of the article, you are free to include or reuse any part of the materials in your thesis or other publications that you write, with citation of the original source in our journal. There is no need to obtain permission.” As Ýrr Mørch, Sofie Snipstad, and Catharina de Lange Davies are co-authors of this paper, explicit copyright permission is not necessary to reuse this figure. All other figures are original figures not published before.

19. Figure 3a/4a/5a: Please remove the commercial names (Shimadzu HPV-X2, CLINIcell, OLYMPUS). Please consider using generic terms.

Commercial names have been replaced by generic terms in Figures 3a, 4a, and 5a.

20. Figure 6a: Please upload a high-resolution fluorescence image.

Figure 6a was made using confocal microscopy. The confocal image was taken at the highest possible resolution. The image resolution was further enhanced to 300 dpi for optimum print quality.

21. Figure 7/8/9: Please include scale bars in all the images of the panel. Please include the details of magnification in the Figure Legends.

Scale bars are added in all images of the panels in Figures 7, 8 and 9.

For Figure 7 and 8 of the bright-field microscopy and fluorescence microscopy respectively, a 2x magnification and 60x objective were used, resulting in a total magnification of 120x. To produce Figure 9, a 20x microscope objective was used. These details have been added to the Figure Legends of Figures 7, 8 and 9.

22. Figure 8: Please label the first image of both “a” and “b” panel. Does the first image denote “0 µs”?

The first images of Figure 8a and 8b indeed denote “0 µs”. Labels have been added to both images.

23. Figure 9: Please label the top left image of panel “b”. Does the first image denote “0 s”?

The first image of Figure 9b indeed denotes “0 s”. A label has been added.

Reviewers' comments:

Reviewer #1:

Manuscript Summary:

In their work, Nawijn et al describe a variety of microscopy techniques to image the behaviour of nanoparticle-microbubble constructs upon ultrasound exposure both in vitro and in vivo. In particular, they use confocal microscopy to structurally characterise the nanoparticle-microbubble constructs, while brigh field or confocal microscopy combined with an ultrasound apparatus are used to monitor the response of the nanoparticle-microbubble constructs to ultrasound exposure in vitro. In addition, the authors show the use of multi-photon microscopy for the intravital imaging of the in vivo fate of nanoparticle-microbubble constructs following ultrasound exposure. Overall, the protocols presented here are well-described and enable an in-depth characterisation of nanoparticle-microbubble constructs in the presence of ultrasound both in vitro and in vivo. As such, this work could be of interest for the scientific community. However, I do have some major concerns that need to be addressed before accepting this manuscript for publication.

We thank the reviewer for the kind words on our paper.

Major Concerns:

Line 166 - Protocol for the production of microbubbles. Since this is a methods paper, I think that the authors should expand the description of the microbubble preparation by adding a brief description of the production of the fluorescently-labeled polymeric nanoparticles. The concentration of the dye should be mentioned, as this could have implications for fluorescence imaging. Similarly, I think it would be good to give an indication of the microbubble stability in the presence of glycerol, as this will affect the amount of time one has to perform imaging.

The nanoparticles were synthesized by the mini-emulsion polymerization method as described previously [3], where the fluorescent dye is encapsulated inside the nanoparticles. A sentence has now been included in step 1.1 to mention this aspect. The concentration of dye for the bubbles described in this paper was 0.21 wt%. This information has now also been added in step 1.1.

We agree with the reviewer that the presence of glycerol could affect the stability of microbubbles. Glycerol was used here to immobilize the microbubbles for the purpose of imaging the shell using confocal microscopy, and not for the other microscopy methods. Single microbubbles were imaged for at least 30 minutes using the confocal microscope at high magnification, and no visible change in the bubble morphology was observed. Furthermore, even if the bubbles underwent a minor depletion, it does not influence the general conclusions we draw on the structure of the shell. A note has now been added in the manuscript after step 2.1.1.4 to reflect this.

My major concern regards the entrapment of the nanoparticles within the protein shell of the microbubbles. Microbubbles have diameters ranging from 1 to 10 um; in order to entrap nanoparticles with diameters of 100-200 nm, the microbubble shell should be at least 210 nm thick, which seems very high compared to common lipid-based shells, which have thicknesses of few nanometers. Most commonly, biotinylated nanoparticles are bound on the surface of biotinylated microbubbles via avidin; in this case, the lipid shell which stabilises the microbubble has a thickness of a few nanometers. Why did the authors choose to entrap the nanoparticles within the casein shell?

We agree with the reviewer that the shell will be thicker when including nanoparticles, this is also what we have shown before, in reference [3]. One benefit of trapping the nanoparticles within the casein shell is that the synthesis of the bubbles is done by a one-step procedure, where all components are mixed and stirred, as opposed to a biotin-avidin binding step, where an additional step of conjugation is required.

What kind of interaction keeps the nanoparticles and casein on the surface of microbubbles?

We see that we need both the casein and the nanoparticles to form stable bubbles. The gas is hydrophobic and the water is hydrophilic, so the casein and the nanoparticles align at the interface. The nanoparticles need to have a certain PEGylation for this to work, which indicates that hydrophobic/hydrophilic interactions are important. However, we think that including these details in the paper is too specific for protein-and-nanoparticle-stabilized microbubbles, as this paper is intended to illustrate how various microscopy methods could be used to characterize and image fluorescently-labeled microbubbles in general.

How stable are the polymeric nanoparticles during the preparation of the nanoparticle-microbubble constructs? I am afraid that you are not entrapping the nanoparticles but just the dye, since lipophilic dyes have been shown to desorb from e.g. lipid-based nanoparticles (e.g. Cauzzo et al. "Following the Fate of Dye-Containing Liposomes In Vitro", International Journal of Molecular Sciences 2020). The authors have previously shown that NR668 is well-retained within poly(butyl cyanoacrylate) nanoparticles. However, the stability of the fluorescently-labelled polymeric nanoparticles in the presence of casein during the preparation of the nanoparticle-microbubble constructs has not been assessed. Could the majority of the nanoparticles be destroyed during the preparation of the nanoparticle-microbubble constructs so that only the lipophilic compound is entrapped within the casein shell?

The stability of the nanoparticles in the presence of the casein during production of the microbubbles in the context of casein-and-polymeric-nanoparticle-stabilized microbubbles has been studied before [4]–[6] and we therefore did not include this stability analysis in the present work where we focus on microscopy imaging methods. That being said, we would like to address the concern of the reviewer on the stability of polymeric nanoparticles. “Stability” can mean several things, including 1) colloidal stability, 2) degradation, or 3) ruptured particles.

If the concern is 1) colloidal stability: From previous work, it has been found that during microbubble synthesis the bubbles are not very stable if only casein is added without nanoparticles. This indicates that the nanoparticles play an important role. The bubbles that we have looked at are stable in the vial for a duration of days. Furthermore, the lumpy shape of the bubbles suggests that particles are present in the shell, as we assume the bubbles are likely more homogenously spherical if the shell of the bubbles consisted of protein alone. We have seen that when casein is added to the nanoparticle solution, some aggregates are formed, which is why we perform a 10-minute sonication step before bubble production as stated in step 1.2 of the manuscript. However, the majority of nanoparticles are still in their free form as has been measured by counting nanoparticles before and after bubble production using a qNano particle sizer.

Regarding 2) degradation of the nanoparticles: The poly(alkylcyanoacrylate) (PACA) nanoparticles start to degrade when the pH is increased. Hence, when we add protein solution (pH 7), the particles will start to degrade, so some degradation and thus leakage of dye, cannot be ruled out. However, note that this is a slow degradation, and since the time from production to analysis is quite short, it is unlikely that this is a concern. We have done cell uptake studies, also at pH 7, and have seen that within the same time frame the dye is not leaking out. Moreover, based on previous experiments where we have looked at leakage of NR668 (also in presence of proteins in cell culture medium) and degradation of the nanoparticles, we do not expect the nanoparticles to degrade during bubble synthesis and that we only entrap dye in the casein shell. This is consistent with various images (SEM images of the bubbles, confocal images of the dye, and SIM image in reference [3]), where we observe patches of dye unevenly distributed throughout the shell. If the dye was to be free, we would expect a more homogeneous distribution within the casein layer. The degradation of microbubbles will be different depending on the type of formulation or bubble construct used, so therefore that aspect is not extensively covered in this paper.

In the case the concern is 3) ruptured particles: We know from SEM imaging of microbubble solutions that the majority of nanoparticles are intact during both sonication and stirring using the dispersion tool.

The authors have also inserted a SEM micrograph of the nanoparticle-microbubble construct. However, the protocol for sample preparation for SEM is not clear: the authors cite their previous work, in which the only information is "NPs and NPMBs were imaged and visually inspected by scanning electron microscopy on either a SEM APREO (NPs) (FEI), or a S(T)EM (NPMBs) (Hitachi). The NPMBs were sputter coated with 5 nm gold prior to imaging.". Since SEM imaging is done on dried samples, I would expect that the nanoparticle-microbubble constructs were dried prior to sputter coating, which would destroy the microbubbles. Therefore, I am not sure that what they report is a nanoparticle-microbubble construct, it could be just a nanoparticle aggregate.
I would really appreciate a more compelling evidence of the successful entrapment of the polymeric nanoparticles within the microbubble shell.

The main reason that the details of the protocol were not included in the manuscript is that we wanted to illustrate how the microscopy methods, other than the ones described in the protocol, can be used for bubble characterization. What we can say is that when imaging bare nanoparticles by SEM their aggregates can have all sorts of shapes, while when imaging nanoparticle-stabilized bubbles the shapes are typically spherical, even though some bubble constructs may have collapsed, see e.g. our previous work [3], [7]. We did not perform an extensive analysis on these images, and therefore we can only give the presented qualitative observations.

Minor Concerns:
there are some grammar mistake or misplaced commas in the text but these can be sorted out at the

proof-reading stage and do not represent a concern.

We thank the reviewer for pointing out the typographical and grammatical errors.

Reviewer #2:

Manuscript Summary:

The goal of this manuscript is to detail the protocol and characterization methods of nanoparticles loaded on microbubble contrast agents. The protocols focus on a microbubble shell containing a fluorescent label. The authors employ nanoparticles loaded with dye as a model drug in this study. The authors discuss microscopy of single microbubbles, along with high-speed imaging of microbubbles to assess bubble dynamics. Fluorescence microscopy is described to visualize release of nanoparticle payload from the bubbles. The extravasation of nanoparticles from microvessels is reported using intravital microscopy. Overall, the manuscript reports characterization of bubble dynamics and therapeutic delivery mechanisms across multiple length scales. The protocols reported are extremely detailed and the manuscript is written lucidly. These comprehensive protocols will be extremely useful for the biomedical ultrasound community.

We thank the reviewer for the nice words and strong recommendation of the protocols.

Major Concerns:

None

Minor Concerns:

I have a few minor comments that I am sure that the authors can address before the publication of this manuscript.

- Page 5, line 217: The authors state that the experiments are conducted with the addition of 50% glycerol to reduce the movement of bubbles. However, it is known that the viscosity of the surrounding media affects both the acoustic response of microbubbles and the rate of gas exchange. Please clarify this point in the manuscript.

We agree with the reviewer that the presence of glycerol can affect the acoustic response and rate of gas exchange of microbubbles. However, in the protocol of this manuscript, glycerol is only used to immobilize the microbubbles for the purpose of imaging the shell using confocal microscopy, not for the other microscopy methods. In the confocal imaging the bubbles are not driven by ultrasound. Regarding the influence of glycerol on the rate of gas exchange, the microbubbles were imaged for at least 30 minutes using the confocal microscope at high magnification, and no visible change in the bubble morphology was observed. A sentence has been added in the manuscript after step 2.1.1.4 to reflect the influence of glycerol on bubble stability and the acoustic response, with reference to [8].

- The protocols for microbubble characterization and nanoparticle release appear to be conducted at room temperature. Temperature affects the ultrasound response of microbubbles. Some discussion on this point is warranted.

All *in vitro* imaging protocols were indeed conducted at room temperature to illustrate the techniques. We agree that temperature has a role in the bubble dynamics and ultrasound response, for example if tested in the more clinically relevant environment at a temperature of 37°C in the presence of cells. If *in vitro* and intravital experiments are to be compared directly, the *in vitro* experiments described in the protocol should be performed at 37°C. Two sentences have now been added to the discussion to reflect this, where we refer to reference [9].

- Discussion: Can the authors comment on the statistical significance of single bubble characterization experiments? In other words, is characterizing dozens or even hundreds of single

microbubbles representative of the bulk population, which can contain of the order of 10^5-10^6 microbubbles/ml in vivo?

Indeed, a selection bias when imaging single microbubbles should be kept in mind. In addition, for the *in vitro* methods described in the protocol the bubbles are not in a free-field environment. However, performing repeated experiments on single bubbles allows for the investigation of the effect of size and removal of the confounding factor that is the size distribution. If we can understand the bubble response as a function of size, while the concentration is not too high to prevent bubble-bubble interactions, we can calculate the response of any arbitrary bubble population. Three sentences have now been added to the discussion to reflect this.

432: What is meant by 10 cycle Gaussian Envelope? Seems to imply that the envelope itself has 10 cycles.

We agree that the above is up for multiple interpretation, so "10-cycle Gaussian envelope" is changed to: "10-cycle Gaussian-tapered pulse" in step 2.3.5.1. A similar change has been made in step 2.2.6.1.

Reviewer #3:

Manuscript Summary:

The authors have developed multi-time-scale microscopy methods applicable for studying ultrasound-triggered drug release. The protocol is valuable and can shed light on the ways studying this drug delivery system. There are some concerns and should be addressed before publication.

We thank the reviewer for the kind words on our paper.

Major Concerns:

How application of those systems, in other words, how about their future application**s** in clinical? What are the limitations and perspectives?

The reviewer is concerned with future applications in the clinic, and the limitations and perspectives of the protein-and-nanoparticle-stabilized microbubbles in particular. Here we would like to emphasize that the described microscopy methods can be applied to any type of fluorescently-labeled microbubbles. Therefore, the perspective and limitations of these specific nanoparticle-labeled microbubbles were not discussed in this paper. We have provided a few general references on clinical translation of therapeutic bubble constructs in the introduction of the manuscript.

Limitations and perspectives of the described protocols were provided in the discussion of the originally submitted manuscript:

"Bright-field microscopy is mainly limited by the imaging framerate and intensity of light sources available, as a higher framerate would give a more detailed time-resolved insight into the bubble dynamics, but requires more intense illumination. In order to study particle release in more detail, the framerate for fluorescence imaging can in principle be increased by increasing the intensity of the laser light. However, absorption of the high-intensity laser light by the fluorescently-labeled microbubbles generates heat, even with high quantum yield dyes. This heat can interfere with the experiments at stake, and in extreme cases induce photo-thermal cavitation [10]. Thus, in practice, there is a limit to the applied laser intensity. On the other hand, intense laser illumination can also be deliberately used to induce particle release from liposomes [11]. Finally, both bright-field and fluorescence microscopy methods provide insight into microbubbles convoluted in a 2D image. If the

research question requires more than 2D imaging, the 3D behavior of the bubbles can be resolved by combining the setup as described in the protocol with a sideview setup for multi-plane imaging [12]."

"A general limitation when performing real-time intravital microscopy is that only a small area of the tissue is imaged, and the penetration depth of the light into tissue is limited. If the imaged vessels contain very few microbubbles and/or nanoparticles within the field of view, little or no information on the nanoparticle behavior and extravasation can be obtained. In addition, because of the limited field of view, a proper alignment between the light and sound paths is crucial. If the ultrasound pressure is high enough to induce bubble destruction, it is also important to choose a pulse repetition frequency that allows fresh bubbles to reperfuse into the field of view between ultrasound pulses. Moreover, the ultrasound will be reflected from the cover glass in the window chamber and the objective, so placing the transducer at an angle is important to reduce reflections as to prevent the formation of standing waves which distort the calibrated pressure field. Another practical issue is that the setup needs to have enough space to mount the ultrasound transducer and waveguide above or below the objective in the microscope setup. The tumors in the dorsal window chamber will have a limited thickness due to the chamber and the cover slip, however if needed, other models could be used. Examples are skinfold tumors, for instance in the mammary fat pad [13], or abdominal intravital imaging of tumors in the various organs [14]. Such tumors can be grown orthotopically in the appropriate microenvironment, and as such present a more clinically relevant case."

We have also added several sentences commenting on the influence of temperature on bubble dynamics, and the relevance of imaging single microbubbles compared to imaging the bulk population.

<u>Minor Concerns:</u>
The language should be polished

We thank the reviewer for the comment, and we have now revised and repolished the manuscript.

What are the advantages compared with other systems?

The advantages of the optical microscopy methods in the protocol of this paper are further discussed in the discussion of the originally submitted manuscript:

"The *in vitro* imaging enables screening of a large number of ultrasound parameters compared to the more complex *in vivo* setups."

"Real-time intravital microscopy during ultrasound exposure is a powerful method to acquire new insight on the vasculature, behavior of microbubbles, nanoparticles, or other molecules (such as dextran in this case) during ultrasound exposure."

"The benefit of combining the range of imaging modalities is the complementary information that can be obtained at different time scales, a feature that is crucial to characterize and optimize the microbubbles for successful delivery and to obtain therapeutic efficacy. This approach is useful to understand the delivery mechanisms for all microbubbles alike, including constructs with fluorescently-labeled nanoparticles and drugs."

We also would like to refer the reviewer to reference [4], also cited in the manuscript, where it was shown that enhanced drug uptake in tumor tissue was achieved by combining these specific casein-and-polymeric-nanoparticles-stabilized microbubbles with ultrasound compared to a systemic administration of a free drug. We also would like to refer to reference [7], where it was shown that

tumor growth can be reduced through co-injection of free drug and nanoparticle-stabilized microbubbles.

References

[1] S. Roovers *et al.*, "The role of ultrasound-driven microbubble dynamics in drug delivery: from microbubble fundamentals to clinical translation," *Langmuir*, vol. 35, no. 31, pp. 10173–10191, 2019.

[2] P. T. Yemane *et al.*, "Effect of Ultrasound on the Vasculature and Extravasation of Nanoscale Particles Imaged in Real Time," *Ultrasound in medicine & biology*, vol. 45, no. 11, pp. 3028–3041, 2019.

[3] Ý. Mørch *et al.*, "Nanoparticle-stabilized microbubbles for multimodal imaging and drug delivery," *Contrast media & molecular imaging*, vol. 10, no. 5, pp. 356–366, 2015.

[4] S. Snipstad *et al.*, "Ultrasound improves the delivery and therapeutic effect of nanoparticle-stabilized microbubbles in breast cancer xenografts," *Ultrasound in medicine & biology*, vol. 43, no. 11, pp. 2651–2669, 2017.

[5] H. Baghirov *et al.*, "Ultrasound-mediated delivery and distribution of polymeric nanoparticles in the normal brain parenchyma of a metastatic brain tumour model," *PloS one*, vol. 13, no. 1, 2018.

[6] M. Fusser *et al.*, "Cabazitaxel-loaded Poly (2-ethylbutyl cyanoacrylate) nanoparticles improve treatment efficacy in a patient derived breast cancer xenograft," *Journal of controlled release*, vol. 293, pp. 183–192, 2019.

[7] S. Snipstad *et al.*, "Sonopermeation Enhances Uptake and Therapeutic Effect of Free and Encapsulated Cabazitaxel," *Ultrasound in Medicine and Biology*, 2021, doi: https://doi.org/10.1016/j.ultrasmedbio.2020.12.026.

[8] R. H. Abou-Saleh *et al.*, "Molecular Effects of Glycerol on Lipid Monolayers at the Gas–Liquid Interface: Impact on Microbubble Physical and Mechanical Properties," *Langmuir*, vol. 35, no. 31, pp. 10097–10105, Aug. 2019, doi: 10.1021/acs.langmuir.8b04130.

[9] H. J. Vos, M. Emmer, and N. de Jong, "Oscillation of single microbubbles at room versus body temperature," in *2008 IEEE Ultrasonics Symposium*, Beijing, China, Nov. 2008, pp. 982–984, doi: 10.1109/ULTSYM.2008.0237.

[10] G. Lajoinie *et al.*, "Ultrafast vapourization dynamics of laser-activated polymeric microcapsules," *Nature communications*, vol. 5, no. 1, pp. 1–8, 2014.

[11] M. Mathiyazhakan *et al.*, "Non-invasive controlled release from gold nanoparticle integrated photo-responsive liposomes through pulse laser induced microbubble cavitation," *Colloids and Surfaces B: Biointerfaces*, vol. 126, pp. 569–574, Feb. 2015, doi: 10.1016/j.colsurfb.2014.11.019.

[12] H. J. Vos, B. Dollet, J. G. Bosch, M. Versluis, and N. de Jong, "Nonspherical Vibrations of Microbubbles in Contact with a Wall—A Pilot Study at Low Mechanical Index," *Ultrasound in Medicine & Biology*, vol. 34, no. 4, pp. 685–688, Apr. 2008, doi: 10.1016/j.ultrasmedbio.2007.10.001.

[13] A. M. Sofias, A. K. O. Åslund, N. Hagen, K. Grendstad, and S. Hak, "Simple and Robust Intravital Microscopy Procedures in Hybrid TIE2GFP-BALB/c Transgenic Mice," *Mol Imaging Biol*, vol. 22, no. 3, pp. 486–493, Jun. 2020, doi: 10.1007/s11307-019-01442-2.

[14] L. Ritsma, E. J. A. Steller, S. I. J. Ellenbroek, O. Kranenburg, I. H. M. Borel Rinkes, and J. van Rheenen, "Surgical implantation of an abdominal imaging window for intravital microscopy," *Nat Protoc*, vol. 8, no. 3, pp. 583–594, Mar. 2013, doi: 10.1038/nprot.2013.026.